Monte Carlo simulation of multiple scattering of elastic waves

Ludovic Margerin, Michel Campillo, Bart van Tiggelen

JOURNAL OF GEOPHYSICAL RESEARCH, VOL. 105, NO. B4, PAGES 7873–7892, APRIL 10, 2000

Monte Carlo simulation of multiple scattering of elastic waves

Ludovic Margerin[1] and Michel Campillo

Laboratoire de Géophysique Interne et Tectonophysique, Observatoire de Grenoble
Université Joseph Fourier, Grenoble, France

Bart Van Tiggelen

Laboratoire de Physique et Modélisation des Systèmes Condensés
Maison des Magistères Jean Perrin CNRS, Grenoble, France

Abstract. We study multiple scattering of elastic waves with a Monte Carlo method. We take into account the mode conversions and the polarization of the S waves. Some important physical parameters relevant to the description of the polarization are recalled, such as the definition and properties of the elastic Stokes vector. We briefly derive the scattering and Mueller matrices, as well as the differential and total scattering cross sections for one spherical inclusion embedded in a homogeneous matrix. The results of the single-scattering problem are used as a building block for multiple scattering. A Monte Carlo method to simulate the propagation of full elastic waves is presented. We pay a special attention to the convergence toward the diffusive regime which exhibits the equilibration of the P and S energy densities. Our simulations show the shear energy to become very rapidly dominant in the coda and the S to P energy density ratio to tend to 10.4 for a Poisson solid, as predicted by the equipartition theorem. However, the typical timescale and length scale to reach equipartition heavily depend on the scattering parameter $k_P a$, where k_P is the P wave number and a is the sphere radius. For Rayleigh scattering ($k_P a \ll 1$) we find a smooth evolution of energy density with time and a slow convergence toward the equilibration, mainly because of the large difference between the P and S scattering mean free paths in this case. On the other hand, for Rayleigh-Gans scattering ($k_P a \sim 1.2, 1.6$) a peak of energy associated with the forward scattered waves is observed, followed by a slow decay according to the diffusion approximation. We find that after only a few mean free times, equipartition is reached in spite of the strong anisotropy of the scattering in this regime. As the scattering parameter $k_P a$ increases, we find that equipartition is again delayed because the transport mean free paths become quite large. We find that a large source-station distance favors a rapid equilibration. This effect is seen to be very pronounced for Rayleigh scatterers. When a source of P waves is considered, the equipartition time can be twice as long as compared with a shear source. The time evolution of the E_P/E_S ratio could be used as a marker for the different scattering mechanisms.

1. Introduction

The propagation of high-frequency elastic waves in the Earth's crust is a complex problem that has been addressed many times in recent years [*Zeng,* 1993; *Sato,* 1994; *Shapiro and Hubral,* 1996; *Sato and Fehler,* 1998]. The complexity stems from the heterogeneity of the crust which involves numerous physical phenomena like reflection and refraction from velocity discontinuities and multiple scattering. One specific feature of elastic wave propagation is that the energy can be transported by coupled compressional (P) and shear (S) waves. Each time a seismic wave encounters boundaries or heterogeneities of the medium, it gives rise to scattered P and S waves which, in turn, will give rise to new scattered P and S waves. This makes the interpretation of high-frequency seismograms rather complex because

[1]Now at Department of Geosciences, Princeton University, Princeton, New Jersey.

Paper number 1999JB900359.
0148-0227/00/1999JB900359$09.00

the coherent P and S wave arrivals from the source are followed by numerous incoherent arrivals which are called coda waves. Most often, the coda is modeled with the acoustic radiative transfer equation. This approximation relies on certain observational and theoretical evidences that the transport of scattered energy should be rapidly dominated by the shear mode [*Dainty and Töksöz,* 1990; *Aki,* 1992; *Papanicolaou et al.*, 1996]. However, even if shear waves are dominant, the P-S mode conversions lead to results different from the acoustic approximation. For example, *Turner* [1998] has shown that in the long-wavelength limit the elastic diffusivity is about 1/3 higher than the pure shear diffusivity.

Several efforts have been made to include mode conversions in the modeling of the seismic coda [*Zeng,* 1993; *Sato,* 1994] relying on some assumptions. Yet, as pointed out several times in the literature [*Ryzhik et al.,* 1996; *Turner,* 1998], some of these assumptions are never fulfilled in practice. For example, scattering of elastic waves is always anisotropic, whatever the value of a/λ, where a is the correlation length of the fluctuations and λ is the wavelength. As in optics, the elastic scattering problem is intrinsically dependent on the state of polarization of the waves, especially for S waves, which are similar to transverse electromagnetic waves. Complete modeling of the multiple scattering of elastic waves should incorporate a description of the polarization. An additional difficulty of elasticity is the interaction of longitudinal and transverse modes. Recently, the radiative transfer (or transport) equations for elastic waves have been obtained independently by *Weaver* [1990] and *Ryzhik et al.* [1996]. These equations can be derived from the wave equation by a rigorous statistical analysis. The conditions of validity of the transport theory are summarized by *Papanicolaou et al.* [1996]. The main condition is that the mean free paths are much larger than the wavelengths, making it possible to neglect interference effects. However, no particular restriction on the a/λ ratio exists, and therefore strong interactions of the waves with the heterogeneities are allowed. The transport equations describe the space and time evolution of the elastic energy as well as the state of polarization of the waves. It has been shown that the evolution of the seismic energy in the coda is ruled by an equilibration law, which states that the ratio of the P to S energy density tends to a constant ratio as time tends to infinity [*Weaver,* 1982, 1990; *Ryzhik et al.* 1996; *Papanicolaou et al.,* 1996]. In the case of a full space this ratio equals $2\alpha^3/\beta^3$, where α and β are the P and S waves velocities, respectively. This result appears immediately by realizing that in the diffusion regime all the volumes of the phase space are equally occupied, consistent with the equipartition theorem. The factor 2 comes from the existence of 2 degrees of freedom for the S waves and only 1 for the P waves. The ratio of the P to S wave speeds cubed comes from the counting of the P and S modes in a given volume of the phase space.

A central question addressed in this paper concerns the required timescale and length scale to reach the diffusion regime in the Earth. In this regime the description of coda waves is greatly simplified. A similar problem has already been studied in acoustics by *Turner and Weaver* [1994a, b, c]. They showed that the time necessary to reach equipartition heavily depends on the scattering mechanism. Only a few mean free times suffice for Rayleigh scattering, while many mean free times are necessary for Mie scattering. Unfortunately, the pioneering results of Turner and Weaver obtained for incident plane waves cannot be transposed directly to seismology. We have to take into account the fact that small earthquakes are almost point-like sources in both space and time. The statistical description of fluctuations in the Earth can be accessed from well log data [*Wu et al.,* 1994] or from geological maps [*Holliger and Levander,* 1992]. For the sake of simplicity, we consider discrete spherical inclusions embedded in a homogeneous matrix.

In this paper we will explain how multiple scattering of elastic waves can be simulated with a Monte Carlo method. For simplicity, only infinite and statistically uniform media are considered, but anisotropy of scattering, polarization, mode conversions, and point-like sources are accurately described. When scattering problems are considered, a complete description of the polarization of the S waves is necessary. Indeed, initially depolarized S waves can become partially polarized by scattering. Moreover, the interaction of S waves with heterogeneities in turn depends on their polarization. In section 2, these problems will be examined.

2. Description of Polarization

2.1. Definition of the Stokes Parameters

In optics, polarized light is represented by a four-element vector, called the Stokes vector, whose components are intensities [*Chandrasekhar,* 1960]. In view of the transverse nature of S waves and electromagnetic waves the definition of the Stokes parameters can readily be transposed from optics to elasticity. To be complete, one additional Stokes parameter is necessary to represent the P waves. Our definition of the elastic Stokes parameters follows the one given by *Turner and Weaver* [1994a]. Let us define a Cartesian reference frame $(\mathbf{x}, \mathbf{y}, \mathbf{z})$ where $\mathbf{z}$ denotes the propagation direction, and let us call ω the central frequency of the waves. The wave displacements can be written at $x = 0, y = 0, z = 0$ (without loss of generality) as

$$\begin{aligned} P(t) &= A_P(t) \exp\left[i\omega t + i\eta(t)\right] \\ S_x(t) &= A_x(t) \exp\left(i\omega t\right) \\ S_y(t) &= A_y(t) \exp\left[i\omega t + i\delta(t)\right], \end{aligned} \tag{1}$$

where δ is the phase difference between the y and x com-

ponent of the S wave, η is a phase shift for the P wave, and $i^2 = -1$. In typical experiments, A_P, A_y, A_z, and δ fluctuate with time t. These fluctuations should obviously be slow compared to the central frequency of the signal. If the wave is polarized, certain constant relations, or correlations, should persist between the phase and amplitude terms of the displacements. This will be expressed mathematically through the Stokes vector:

$$\mathbf{S} = (I_P, I_{S_x}, I_{S_y}, U, V), \tag{2}$$

where

$$I_P = \langle \frac{\rho\omega^2\alpha}{2} A_P^2 \rangle \tag{3a}$$

$$I_{S_x} = \langle \frac{\rho\omega^2\beta}{2} A_x^2 \rangle \tag{3b}$$

$$I_{S_y} = \langle \frac{\rho\omega^2\beta}{2} A_y^2 \rangle \tag{3c}$$

$$U = \langle \rho\omega^2\beta A_x A_y \cos\delta \rangle \tag{3d}$$

$$V = \langle \rho\omega^2\beta A_x A_y \sin\delta \rangle, \tag{3e}$$

where ρ is the density of the medium and α and β are the P and S wave velocities, respectively. The angle brackets indicate that the time average is taken over a large number of periods. The parameters defined in (3a)-(3c) are just the intensities carried by the wave when measured along the three axes of the reference frame. The last two parameters, U and V, measure the cross correlations between the x and y components of the shear wave. We note that the four parameters (3b)-(3e) contain information about the total intensity, the degree of polarization, the ellipticity, and the plane of polarization of S waves, as in optics. For future developments we will give the relation between the Stokes parameters and the ellipticity and azimuth of the polarization plane in the simple case of elliptical polarization. The azimuth $-\pi/2 < \chi < +\pi/2$ is defined as the angle between the major axis of the ellipse and the x axis. The ellipticity $\tan|\epsilon| \leq 1$ is defined as the ratio of length of the minor to the major axis; $\epsilon > 0$ corresponds to a right-handed ellipse, and $\epsilon < 0$ corresponds to a left-handed one. We have

$$\tan 2\chi = \frac{U}{I_{S_x} - I_{S_y}} \tag{4}$$

$$\sin 2\epsilon = \frac{V}{I_{S_x} + I_{S_y}}. \tag{5}$$

2.2. Properties of the Stokes Parameters

A useful property is that independent Stokes vectors are additive. "Independent" here means that the waves, whose Stokes parameters are added, do not obey any phase relations [*Chandrasekhar,* 1960]. The Stokes parameters are subject to the inequality

$$(I_{S_x} + I_{S_y})^2 \leq (I_{S_x} - I_{S_y})^2 + U^2 + V^2. \tag{6}$$

The equality applies when the wave is elliptically polarized. In this case, only three parameters are necessary to characterize the polarization ellipse. Another relation that we will need is the transformation of the Stokes parameters when the coordinate system is rotated an angle ϕ around the z axis. One can show that the Stokes vector $\mathbf{S}$ in the new coordinate system is related to the Stokes vector $\mathbf{S_0}$ in the old coordinate system by the matrix relation [see *Turner and Weaver,* 1994a]:

$$\mathbf{S} = \mathbf{L}\mathbf{S_0}. \tag{7}$$

The expression of the 5×5 matrix $\mathbf{L}$ can be found in Appendix A. It is worth noting that V, I_P, and $I_S = I_{S_x} + I_{S_y}$ are invariant under this rotation. Indeed, V corresponds to the decomposition of the wave on the basis of the right and left circular polarization.

3. Scattering by One Sphere

To study the multiple scattering of elastic waves, we consider a very simple model composed of randomly distributed spherical inclusions in a homogeneous matrix. The spherical inclusions are of the same nature and show a small contrast of wave speeds and density with the reference medium. We assume that the wave speeds and the density are equally perturbed. The choice of spherical scatterers introduces symmetry relations that greatly simplify the problem. The first step is to calculate all the physical quantities relevant to the description of scattering by a single sphere. Then these results will be used as a building block for multiple scattering. The scattering of elastic waves by one sphere has been largely studied, and many references exist in the literature [*Ying and Truell,* 1956; *Einspruch et al.,* 1960; *Wu and Aki,* 1985a; *Korneev and Johnson,* 1993a, b, 1996]. For the sake of simplicity, we shall follow the approach of *Wu and Aki* [1985a], who calculated the field scattered by one sphere using the Born approximation. In this approximation the elastic inclusion is decomposed in infinitesimal volumes which are considered as independent Rayleigh scatterers. The total scattered field is written as a sum of partial waves emitted by each fraction of the whole inclusion. Thereby, the Born approximation neglects interactions between infinitesimal volumes and holds good as long as $k_{P,S}a|m-1| \ll 1$, where $k_{P,S}$ is the P or S wave number, a is the radius of the sphere, and $m = \alpha/\alpha_0$ or $m = \beta/\beta_0$ is the value of the ratio of the wave speeds inside and outside the sphere. As in the electromagnetic literature [*Van de Hulst,* 1981], we will term this scattering mechanism "Rayleigh-Gans" scattering. The results of *Wu and Aki* [1985a] written in a slightly modified form will be our starting point to derive some physical quantities of interest such as the scattering and Mueller matrices and the differential and integrated scattering cross sections.

3.1. Scattering and Mueller Matrices

We consider a plane wave propagating in the $\mathbf{z}$ direction, incident on a sphere centered at the origin of the Cartesian reference frame $(\mathbf{x}, \mathbf{y}, \mathbf{z})$. The scattered wave propagates in the $\mathbf{z}'$ direction, at an angle Θ with $\mathbf{z}$. The plane containing $\mathbf{z}$ and $\mathbf{z}'$ is called the scattering plane. To derive the scattering matrix, we choose the following convention (see Figure 1): the incident Stokes parameters are expressed in the $(\mathbf{r}, \mathbf{l}, \mathbf{z})$ Cartesian frame where $\mathbf{r}$ and $\mathbf{l}$ denote the directions perpendicular and parallel to the scattering plane, respectively.

Similarly, the Stokes parameters of the scattered wave are expressed in the $(\mathbf{r}', \mathbf{l}', \mathbf{z}')$ Cartesian frame where the same convention is assumed. We find that the incident and scattered Stokes vectors $\mathbf{S}_{\text{inc}}$, $\mathbf{S}_{\text{sc}}$ are related by

$$\mathbf{S}_{\text{sc}} = \frac{1}{r^2}\mathbf{F}\mathbf{S}_{\text{inc}}, \tag{8}$$

where r is the distance from the center of the inclusion to the observer and $\mathbf{F}$ is the scattering matrix:

$$\mathbf{F} = \frac{1}{16\pi^2}\begin{pmatrix} k_P^4\gamma_1^2(\Theta)f_{PP}^2(\Theta) & 0 & \frac{\alpha}{\beta}k_P^4\gamma_3^2(\Theta)f_{SP}^2(\Theta) & 0 & 0 \\ 0 & k_S^4\gamma_4^2(\Theta)f_{SS_r}^2(\Theta) & 0 & 0 & 0 \\ \frac{\beta}{\alpha}k_S^4\gamma_2^2(\Theta)f_{PS}^2(\Theta) & 0 & k_S^4\gamma_4^2(\Theta)f_{SS_l}^2(\Theta) & 0 & 0 \\ 0 & 0 & 0 & k_S^4\gamma_4^2(\Theta)f_{SS_l}(\Theta)f_{SS_r}(\Theta) & 0 \\ 0 & 0 & 0 & 0 & k_S^4\gamma_4^2(\Theta)f_{SS_l}(\Theta)f_{SS_r}(\Theta) \end{pmatrix} \tag{9}$$

where k_P and k_S are the P and S wave numbers, respectively. The functions $f_\star(\Theta)$ and $\gamma_\star(\Theta)$ come out of the Born approximation with the subscript star denoting any of these functions. The functions $f_\star$ correspond to Rayleigh scattering and the functions $\gamma_\star$ are shape factors that appear for scatterers of finite size. In Appendix B we explain our choice of conventions and how these functions can be recovered from the work of *Wu and Aki* [1985a]. The matrix $\mathbf{F}$ depends on Θ only as required by the rotational symmetry (see *Van de Hulst* [1981] for details). From the structure of the matrix $\mathbf{F}$, it can be inferred that for an elliptically polarized incident wave the scattered wave will remain elliptically polarized. This means that depolarization can occur in multiple scattering only.

The scattering matrix is not convenient to deal with multiple scattering, since it is referred to a local frame. For the purpose of our simulation we will find it convenient to know how a beam of energy propagating in a direction of space (θ', ϕ') contributes to a beam propagating in an other direction of space(θ, ϕ), where $(\theta^{(\prime)}, \phi^{(\prime)})$ refer to the usual definition of polar coordinates in a global reference frame $(O, \mathbf{x}, \mathbf{y}, \mathbf{z})$. Moreover, a convention must be adopted for the analysis of the polarization of S waves. Following *Turner and Weaver* [1994a], the Stokes vector will be written in the basis $(\mathbf{u}_\theta, \mathbf{u}_\phi, \mathbf{p})$ composed of three unit vectors in the direction of increasing θ, increasing ϕ and in the propagation direction respectively (see Figure 2). With these conventions the incident and scattered Stokes vectors $\mathbf{S}_{\text{inc}}$ and $\mathbf{S}_{\text{sc}}$ are related by $\mathbf{S}_{\text{sc}} = \mathbf{P}\mathbf{S}_{\text{inc}}$, where the Mueller matrix $\mathbf{P}$ can be deduced from the scattering matrix $\mathbf{F}$ after carrying out the necessary rotations (see *Chandrasekhar* [1960] for electromagnetic waves and *Turner and Weaver* [1994a] for elastic waves). Upon introducing i_1, the dihedral angle between the plane containing the directions Oz and (θ', ϕ') and the scattering plane, i_2, the dihedral angle between the scattering plane and the plane containing the directions Oz and (θ, ϕ) (see Figure 2), the Mueller matrix reads

$$\mathbf{P}(\theta, \phi; \theta', \phi') = \mathbf{L}(i_2 - 3\pi/2)\mathbf{F}(\Theta)\mathbf{L}(i_1 + \pi/2). \tag{10}$$

The rotation through i_1 brings the incident basis in the scattering plane and enables us to use relation (8). The rotation through i_2 ensures that the outgoing Stokes vector is referred to the basis $(\mathbf{u}_\theta, \mathbf{u}_\phi, \mathbf{p})$. The expression of the Mueller matrix for a spherical elastic inclusion is given in Appendix C. From the structure of this matrix we see that the parameter V decouples and that linearly polarized S waves give rise to scattered waves that are still linearly polarized. This property will be helpful when considering the numerical simulation.

3.2. Scattering Cross Sections

We shall first consider the differential cross sections, which contain all the information about the angular dependence of the scattered flux. They are defined as the ratio of the energy scattered in the space direction (Θ, Φ) (see Figure 1) per unit time and per unit solid angle by the spherical inclusion to the energy per unit area and unit time carried by the incident wave [*Sato and Fehler*, 1998]. These cross sections clearly depend on the polarization of incident and scattered waves. In the following, we will consider linearly polarized S waves only for simplicity, but our results can easily be generalized to any type of polarization. From the solution of the scattering problem given by *Wu and Aki* [1985a] and Appendix B, we find

$$\frac{d\sigma_{PP}}{d\Omega} = \frac{k_P^4}{16\pi^2}\gamma_1^2(\Theta)f_{PP}^2(\Theta) \tag{11a}$$

$$\frac{d\sigma_{PS}}{d\Omega} = \frac{k_S^4\beta}{16\pi^2\alpha}\gamma_2^2(\Theta)f_{PS}^2(\Theta) \tag{11b}$$

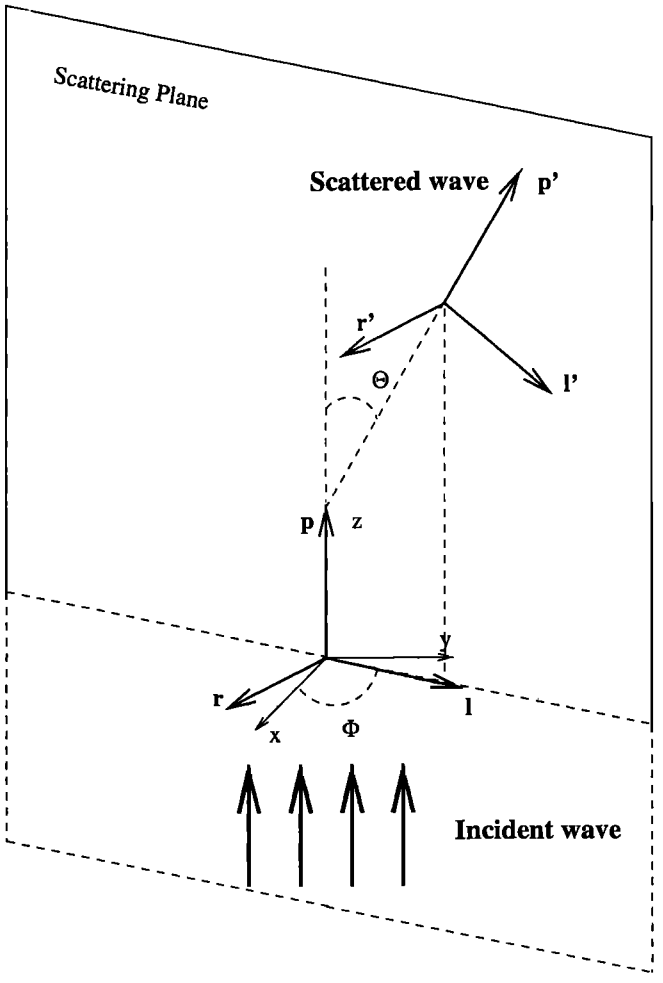

Figure 1. Sketch of the convention used to derive the scattering matrix.

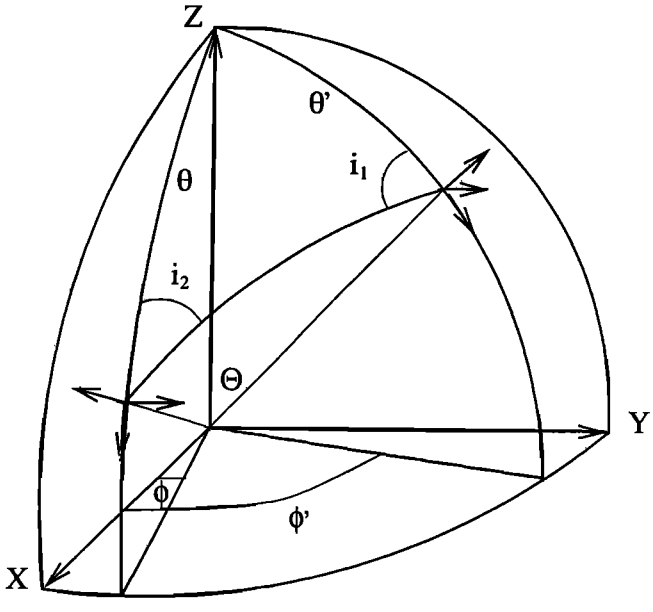

Figure 2. Sketch of the convention used to derive the Mueller matrix. The i_1 denotes the dihedral angle between the incident and scattering planes, while i_2 denotes the dihedral angle between the scattering and outgoing planes. Θ is the scattering angle.

$$\frac{d\sigma_{SP}}{d\Omega} = \frac{k_P^4 \alpha}{16\pi^2\beta}\gamma_3^2(\Theta) f_{SP}^2(\Theta)\cos^2\Phi \quad (11c)$$

$$\frac{d\sigma_{SS}}{d\Omega} = \frac{k_S^4}{16\pi^2}\gamma_4^2(\Theta)(f_{SS_l}^2(\Theta)\cos^2\Phi + f_{SS_r}^2(\Theta)\sin^2\Phi). \quad (11d)$$

In (11a)-(11d), Θ is the angle between the incident and scattered directions and Φ is the angle between the scattering plane and the polarization plane of the S wave, which contains both the propagation and wave displacement directions. For incident S wave polarized in the $\mathbf{x}$ direction, the polarization plane is merely $(\mathbf{x}, \mathbf{z})$ and Φ is the usual azimuthal angle. The symbol $d\Omega$ indicates that the differential cross sections are defined per unit solid angle. We adopt this notation because it is most commonly used in optics. As has already been noted by *Papanicolaou et al.* [1996] and *Turner* [1998], the angular distribution of scattered energy is never isotropic, even in the low-frequency limit $k_{P,S}a \ll 1$ or Rayleigh regime.

The integrated scattering cross sections Σ_{MN}, with $M, N = S, P$, are obtained by integrating the differential cross sections over the solid angle. In the case of incident S waves the total cross sections for a spheri-

cal inclusion do not depend on the polarization because of the symmetry of the scatterer [*Van de Hulst,* 1981]. In the intermediate frequency regime $ka \simeq 1$, the cross sections can be evaluated numerically. The accuracy of our computations has been checked, using the results presented by *Korneev and Johnson* [1993b]. In the Rayleigh regime the scattering cross sections can be computed analytically and are given in Appendix D. It is important to note that according to the definition of the scattering cross sections and the symmetry of the function f_{SP} and f_{PS}, a relation exists between Σ_{SP} and Σ_{PS}:

$$\Sigma_{PS} = 2\frac{\alpha^2}{\beta^2}\Sigma_{SP}, \tag{12}$$

independent of the scattering mechanism. As has been explained by *Aki* [1992], this relation finds its origin in the reciprocity of the Green functions. The same relation has been obtained by *Papanicolaou et al.* [1996] for a continuous random medium. The reciprocity argument of Aki also holds for scatterers of more complicated shape, making (12) a fundamental relation. For completeness, we recall the definition of the shear and compressional waves mean free paths, denoted by l_S and l_P, respectively:

$$l_S = \frac{1}{n}(\Sigma_{SP} + \Sigma_{SS}) = \frac{\Sigma_S}{n}, \tag{13a}$$

$$l_P = \frac{1}{n}(\Sigma_{PS} + \Sigma_{PP}) = \frac{\Sigma_P}{n}, \tag{13b}$$

where n is the density of scatterers.

4. Diffusion of Elastic Waves

Recently, *Turner* [1998] made a summary of theoretical work done on multiple scattering of elastic waves. For our purpose, it is important to recall some results concerning the diffusion of elastic waves. It has first been shown by *Weaver* [1990] that the propagation of elastic waves in inhomogeneous media could be described by a radiative transfer equation, which is a coupled equation for the five Stokes parameters described above. For large lapse times the equation of radiative transfer can be turned into a simple diffusion equation for the total energy density (E) of the P and S modes. It is remarkable that such a simple scalar equation is able to describe the evolution of the seismic energy. Since the diffusion theory is much easier to use than the full radiative transfer equation, it would be very interesting to know what are the typical timescale and length scale necessary to reach the diffusive regime. In this regime the total energy density E for a point source in both space and time in an infinite nondissipative medium reads

$$E(R,t) = \frac{1}{(2\sqrt{\pi D t})^3}\exp\left(-R^2/4Dt\right), \tag{14}$$

where t is the lapse time, R is the source station distance, and D is the diffusion constant of elastic waves:

$$D = \frac{1}{1+2K^3}\left(\frac{\alpha l_P^\star}{3} + 2K^3\frac{\beta l_S^\star}{3}\right). \tag{15}$$

The variables α, β are the P and S wave speeds, respectively, and $K = \alpha/\beta$ is the P to S wave speed ratio. A crucial point is the definition of the transport mean free paths $l_P^\star$ and $l_S^\star$ appearing in (15). In order to cope with discrete scatterers we have to modify slightly the definitions given by *Turner* [1998] and obtain

$$l_P^\star = \frac{1}{n}\frac{\Sigma_S - \Sigma_{SS}^\star + \Sigma_{PS}^\star}{(\Sigma_P - \Sigma_{PP}^\star)(\Sigma_S - \Sigma_{SS}^\star) - \Sigma_{PS}^\star\Sigma_{SP}^\star} \tag{16a}$$

$$l_S^\star = \frac{1}{n}\frac{\Sigma_P - \Sigma_{PP}^\star + \Sigma_{SP}^\star}{(\Sigma_P - \Sigma_{PP}^\star)(\Sigma_S - \Sigma_{SS}^\star) - \Sigma_{PS}^\star\Sigma_{SP}^\star}, \tag{16b}$$

where the following notations have been introduced:

$$\Sigma_{MN}^\star = \int_{4\pi}\frac{d\sigma_{MN}(\cos\Theta)}{d\Omega}\cos\Theta d\cos\Theta d\Phi \qquad M,N = P,S \tag{17}$$

and n is the density of scatterers. The $\Sigma_{M,N}^\star$ are the averages of the cosine of the scattering angle, weighted by the differential cross section. The definition of the transport mean free paths in terms of the $\Sigma_{M,N}^\star$ are more complicated than in the acoustic case. The exact results of the diffusion theory will be useful in checking the accuracy of our numerical simulations.

Another relation of importance is the value of the equilibration ratio of the P to S energy density, shown to be independent of the details of the scattering [*Ryzhik et al.,* 1996],

$$\frac{E_P}{E_S} = \frac{1}{2}\left(\frac{\beta}{\alpha}\right)^3. \tag{18}$$

We finally comment on the definitions of the wave speeds appearing in the diffusion theory. It is now well established that in the case of very strong scattering, we have to distinguish between the phase and group velocities of a pulse and the transport velocity appearing in the definition of the diffusion constant [*Lagendijk and Van Tiggelen,* 1996]. It has been shown that for resonant scatterers the transport velocity can be reduced by a factor of 10 compared to the phase velocity. Since we consider scatterers away from resonances, the difference between the phase, group, and transport velocity becomes immaterial.

5. Monte Carlo Simulation

In recent years, the Monte Carlo method has been used to model the propagation of high-frequency seismic waves in the Earth's lithosphere. Starting from infinite space models [*Gusev and Abubakirov,* 1987; *Abubakirov and Gusev,* 1990; *Hoshiba,* 1991], the most recent models [*Hoshiba,* 1997; *Margerin et al.* 1998] have also in-

cluded depth dependence of wave velocity and scattering mean free path, yet retain the acoustic approximation. In the simple case of neutrons or depolarized photons it can be rigorously established that Monte Carlo simulations are, in fact, "exact" solutions of the radiative transfer equation. "Exact" here means that in the limit of a very large number of independent simulations the Monte Carlo solution converges to the exact solution of the radiative transfer equation. Proofs are given by *Lux and Koblinger* [1991]. To the best of our knowledge, no such formal proof exists in the case of elastic waves. However, there are some numerical and theoretical evidences that Monte Carlo methods are able to solve coupled systems of integro-differential equations such as the elastic transport equations [*Marchuk et al.*, 1980].

Our scheme is a one-to-one simulation of the transfer process and is therefore restricted to the same assumptions. Scatterers are supposed to be independent, that is, we neglect recurrent scatterings. In more technical words, the transport equation applies only when the mean free path is large enough compared to the wavelength. The mathematical assumptions underlying the transport approach are described by *Ryzhik et al.* [1996] and the transition from transport to localization phenomena is discussed by *Van Tiggelen* [1999]. In this section we will generalize the Monte Carlo method to include mode conversions. The problem of boundary reflections and nonuniform mean free path will not be discussed in this paper. Instead, we will emphasize the elastic aspects and the time-dependent propagation.

5.1. Outline of the Simulation

The Monte Carlo method requires three steps, which are schematically depicted in Figure 3. First, the random walk of "particles" representing seismic wave packets is simulated. The path length distribution is given by an exponential probability law. Second, at each scattering event the energy contribution of the particle is calculated in terms of probability at different receivers. Finally, the average of all the random walk results is calculated to obtain the time evolution of the seismic energy at different positions of space (see, e.g., *Hoshiba* [1991] for a clear description of the basic method).

Our treatment follows the one used for anisotropic scattering of acoustic waves [*Hoshiba,* 1995]. To describe the particle, we use the following quantities: (1) vectors $\mathbf{I} = (x_I, y_I, z_I)$ and $\mathbf{p} = (p_x, p_y, p_z)$ to determine the position and propagation direction, respectively, in a Cartesian global reference frame $(\mathbf{x}, \mathbf{y}, \mathbf{z})$, (2) travel time of the particle since the emission at the source is stored in a scalar T, and (3) to allow for absorption in the medium, a weight $0 < w \leq 1$ is assigned to the particle. In the following, we will consider nondissipative media only. For elastic waves, additional information is required: (1) the polarization M of the wave (P or S) and (2) for S waves the Stokes vector $\mathbf{S} = (I_{S_1}, I_{S_2}, U, V)$ that describes the polarization. In our simulation the

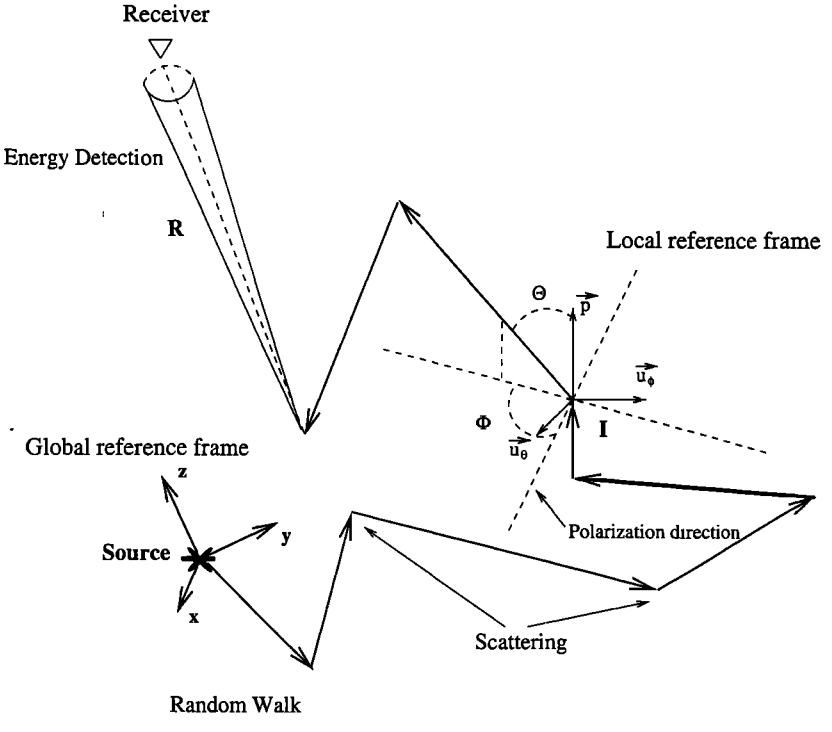

Figure 3. Schematic picture of the Monte Carlo simulation. The particle starts at a point source and makes a random walk in the medium. At each scattering, the choice of the new mode, propagation direction, and path length is made; the energy contribution of the particle is also calculated at the receiver.

Stokes vector is written with the same convention as the one used for the Mueller matrix. For example, if a particle propagates in the direction $\mathbf{p}$, the shear components of the displacement are analyzed in the basis $(\mathbf{u}_\theta, \mathbf{u}_\phi, \mathbf{p})$, where $\mathbf{u}_\theta$ and $\mathbf{u}_\phi$ denote unit vectors in the direction of increasing θ and ϕ, respectively, in the global reference frame (see Figures 2 and 3).

5.2. Random Walk

During its random walk the particle changes its direction of propagation and may also change polarization. We will assume an isotropic and point-like source radiation in both space and time of either P or S waves. For S waves we make the additional assumption that they are initially linearly polarized. Since both P and linearly polarized S waves scatter into linearly polarized S waves as explained earlier, our last assumption implies that the particle is fully linearly polarized during all the propagation in the medium. Thus the depolarization of S waves can only occur when summing the contributions of many independent particles. This fact greatly simplifies the selection of the propagation direction after scattering since we will only have to consider the scattering of P waves or linearly polarized S waves.

5.2.1. Distance between collisions. Between two collisions, the wave will propagate ballistically on a length L, which is determined by the exponential probability distribution $(1/l_M)\exp(-L/l_M)$, where $M = P, S$ denotes the polarization of the wave.

5.2.2. Scattering of elastic waves. When a collision occurs, one must determine the new polarization and propagation direction after scattering according to the scattering cross sections. We use the methods developed by *Collins et al.* [1972] to study the propagation of light through the atmosphere and the methods of *Heiderich* [1995] and *Heiderich et al.* [1997] to cope with light scattering in nematic liquid crystals. Light propagation in nematics bears some important resemblances with elastic wave propagation. Among these similarities, one can cite the existence of two modes of propagation (ordinary and extraordinary) with two different wave speeds and the anisotropy of the differential scattering cross sections. In elastic case, the joint probability distribution of the polarization $M_{\rm sc}$ and of the propagation direction $(\cos\Theta, \Phi)$ after scattering reads

$$P(M_{\rm inc}|M_{\rm sc}, \cos\Theta, \Phi) = \frac{\frac{d\sigma}{d\Omega}(M_{\rm inc}|M_{\rm sc}, \cos\Theta, \Phi)}{\sum_{M_{\rm inc}} \int_{4\pi} \frac{d\sigma}{d\Omega}(M_{\rm inc}|M_{\rm sc}, \cos\Theta, \Phi) d\cos\Theta d\Phi}. \quad (19)$$

$P(M_{\rm inc}|M_{\rm sc}, \cos\Theta, \Phi)$ denotes that the probability distribution is parameterized by the incident polarization $M_{\rm inc}$. The core of the Monte Carlo simulation consists in accurately simulating this probability distribution. As in the case of anisotropic scattering of scalar waves, the polar and azimuthal angles (Θ, Φ) are selected in a local frame (see Figure 3). A rotation of coordinates provides the new propagation directions in the global coordinate system. In the case of incident P waves the angle Φ is equidistributed over $[0, 2\pi]$. In the case of incident S waves, Φ denotes the angle between the plane of polarization and the scattering plane. From the definition of the probability distribution (19) we conclude that the variables $M_{\rm sc}, \cos\Theta$, and Φ are not independent. This is an additional complication of the Monte Carlo simulation for elastic waves. To overcome this difficulty, we will rewrite (19) as a product of conditional probability distributions:

$$P(M_{\rm inc}|M_{\rm sc}, \cos\Theta, \Phi) = P(M_{\rm inc}|M_{\rm sc}) \times P(M_{\rm inc}, M_{\rm sc}|\cos\Theta) P(M_{\rm inc}, M_{\rm sc}, \cos\Theta|\Phi), \quad (20)$$

where the following notations have been introduced:

$$P(M_{\rm inc}|M_{\rm sc}) = \frac{\int_{4\pi} \frac{d\sigma}{d\Omega}(M_{\rm inc}|M_{\rm sc}, \cos\Theta, \Phi) d\cos\Theta d\Phi}{\sum_{M_{\rm sc}} \int_{4\pi} \frac{d\sigma}{d\Omega}(M_{\rm inc}|M_{\rm sc}, \cos\Theta, \Phi) d\cos\Theta d\Phi} \quad (21)$$

is the conditional probability of the mode $M_{\rm sc}$,

$$P(M_{\rm inc}, M_{\rm sc}|\cos\Theta) = \frac{\int \frac{d\sigma}{d\Omega}(M_{\rm inc}, M_{\rm sc}|\cos\Theta, \Phi) d\Phi}{\int_{4\pi} \frac{d\sigma}{d\Omega}(M_{\rm inc}, M_{\rm sc}|\cos\Theta, \Phi) d\cos\Theta d\Phi} \quad (22)$$

is the conditional probability of the cosine of the scattering angle $\cos\Theta$, and

$$P(M_{\rm inc}, M_{\rm sc}, \cos\Theta|\Phi) = \frac{\frac{d\sigma}{d\Omega}(M_{\rm inc}, M_{\rm sc}, \cos\Theta|\Phi)}{\int_{4\pi} \frac{d\sigma}{d\Omega}(M_{\rm inc}, M_{\rm sc}, \cos\Theta|\Phi) d\Phi}, \quad (23)$$

is the conditional probability of the angle Φ. Note that in these equations, the vertical bar separates the known parameters from those that have to be randomly selected. Equation (20) decomposes the joint probability distribution as a product of conditional probability distributions. At this point, three independent numbers $\epsilon_1, \epsilon_2, \epsilon_3$, uniformly distributed between $]0, 1[$ are randomly generated. First, we select the mode of the scattered wave $M_{\rm sc}$, which depends on the mode of the incident wave. For example, in the case of an incident S wave the probability to be converted is $P_{\rm conv} = \Sigma_{SP}/(\Sigma_{SS} + \Sigma_{SP})$, and the probability to keep the same mode is $1 - P_{\rm conv} = \Sigma_{SS}/(\Sigma_{SS} + \Sigma_{SP})$ consistent with (21). Thus, if ϵ_1 is smaller than $P_{\rm conv}$, the wave is converted; otherwise, it keeps its original mode. Once the mode of the scattered wave is known, we select the value of $\cos\Theta$ with the usual inverse distribution function method [*Lux and Koblinger,* 1991]:

$$\epsilon_2 = \int_0^{\cos\Theta} P(M_{\rm inc}, M_{\rm sc}|\cos\Theta')d\cos\Theta' \qquad (24)$$

Since the angular dependence is too complicated to find $\cos\Theta$ as an explicit function of ϵ_2, we divide the $[-1,1]$ interval into subintervals of equal probability such that

$$\int_{\cos\Theta_{i-1}}^{\cos\Theta_i} P(M_{\rm inc}, M_{\rm sc}|\cos\Theta')d\cos\Theta' = \frac{1}{q}, \qquad (25)$$

where q denotes the number of intervals and $i \in [0,q]$. These values are stored in a table which is calculated once at the beginning of the simulation, from which we can select randomly the value of $\cos\Theta$. Finally the angle Φ is selected with the same method:

$$\epsilon_3 = \int_0^{\Phi} P(M_{\rm inc}, M_{\rm sc}, \cos\Theta|\Phi')d\Phi'. \qquad (26)$$

Once the propagation direction of the scattered wave is known in the local coordinate system, a rotation provides the propagation direction of the particle ($\mathbf{p_x}$,$\mathbf{p_y}$, $\mathbf{p_z}$) in the global coordinate system. Then, using the Mueller matrix, the Stokes vector of the scattered wave can be calculated, enabling us to also keep track of the orientation of the polarization in the global reference frame. For further details, we refer to *Heiderich et al.* [1997]. It is worth mentioning that using a very similar method for polarized light, *Collins et al.* [1972] have shown good agreement between the Monte Carlo computations and solutions of the radiative transfer equation obtained with other numerical methods.

5.3. Energy Detection

The step of the simulation dealing with energy detection is very similar to the acoustic case except that the particle contributes to the P and S modes at each scattering event. We refer to *Hoshiba* [1995] for the details of the Monte Carlo simulation for anisotropic scattering and just give the expressions of the probabilities for the elastic case:

$$E_{M_{\rm sc}} = \frac{P(M_{\rm inc}|M_{\rm sc}, \cos\Theta, \Phi)\exp(-R_{sd}/l_{M_{\rm sc}})}{R^2 v_{M_{\rm sc}} dt} \qquad (27)$$

where $v_{M_{\rm sc}}$ denotes the wave speed of the scattered mode $M_{\rm sc}$. R_{sd} is the distance between the scattering site and the detector, and dt is the discretization step of time. The energy contributions of the particle at each scattering event are stored in a vector $\rho_M(t)$, which is the discrete version of the energy density as a function of time. Finally, all random walk results are averaged to provide an estimate of the energy density of each mode.

6. Numerical Tests

We expect our numerical solutions to lie between the single-scattering (SSc) and diffusion approximations. The SSc approximation for elastic waves has been studied in detail by *Sato* [1984] and *Wu and Aki* [1985b]. Using the formulas of *Sato* [1984] (equations (68a)-(68d)) and the diffusion theory outlined in this paper, we have compared the decay of the total energy density in the SSc and diffusion approximations, against our numerical results. This comparison is plotted in Figures 4a and 4b for an isotropic source of linearly polarized shear waves because seismic sources mainly release shear energy. In all the simulations presented in this paper the mean free path of the shear waves is $l_S = 30$ km. According to the definition of the mean free paths (see equations (13a), (13b), (16a), (16b)), the value of l_S can be adjusted by changing the density of scatterers in the medium. Note that the ratios l_P/l_S or $l_P^\star/l_S^\star$ do not depend on the density of scatterers. Since the time axis

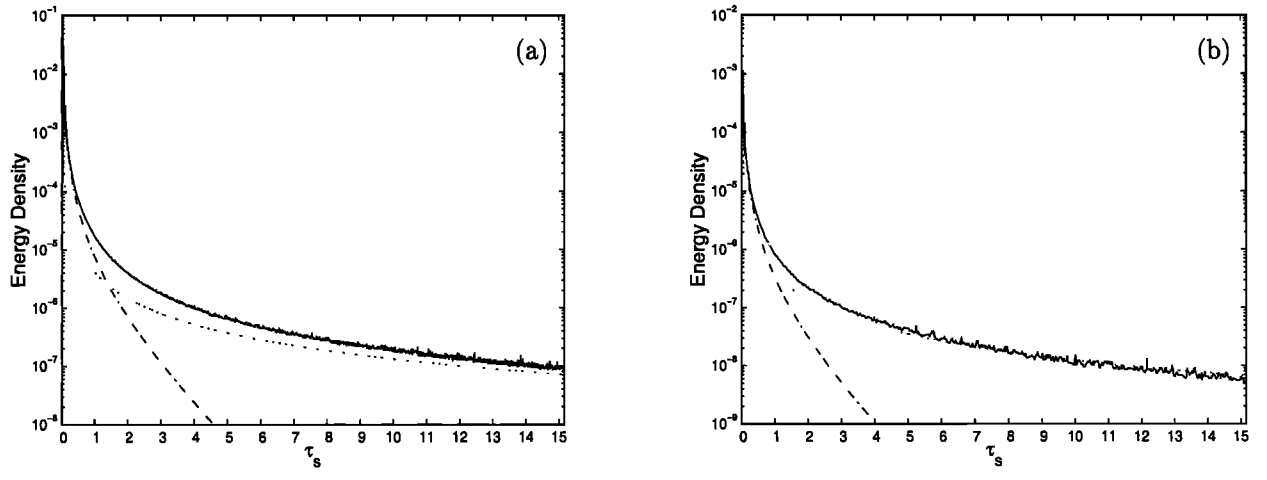

Figure 4. Comparison of the Monte Carlo simulation (solid) with the single-scattering (dash-dotted) and diffusion approximation (dotted) for an isotropic source of S waves close to the receiver for (a) Rayleigh regime and (b) Rayleigh-Gans regime.

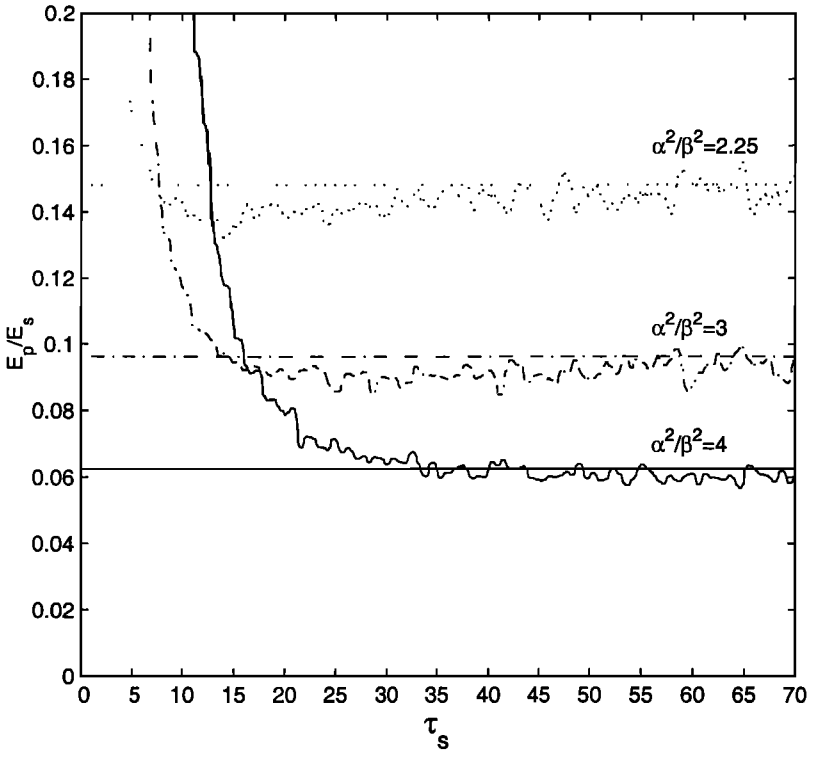

Figure 5. P to S energy ratio as a function of time for different values of the ratio of wave speeds α/β. The Monte Carlo solutions exhibit characteristic ripples. The theoretical asymptotic value of the equilibration ratio is also plotted. Time unit is the mean free time of the shear waves.

is normalized with respect to the shear mean free time, the choice of l_S is completely arbitrary and determines only the absolute value of the energy density, which is not a parameter of interest in our case.

In Figure 4a we consider Rayleigh scatterers, i.e., with size much smaller than the wavelength ($k_{P,S}a \ll 1$). In Figure 4b, we consider Rayleigh-Gans scatterers whose size is comparable to the wavelength ($k_P a = 2$). As will be explained latter, these two regimes strongly differ in their scattering characteristics. For both size of scatterers, at short times, we find that our solution perfectly matches the SSc asymptotic and as time increases, our solution approaches the solution of the diffusion equation. In addition, our Monte Carlo simulation describes the intermediate multiple-scattering regime. After one mean free time, the single-scattering and full numerical solutions start to diverge strongly, which shows that multiple-scattering effects become important. It is also clear that after a few mean free times the diffusion approximation is much closer to the full numerical solution than the SSc approximation.

Another strong constraint on our numerical results is the equilibration ratio of the P to S energy densities, as given in (18). We have performed a series of simulations in the Rayleigh regime with $\alpha/\beta = 1.5, \sqrt{3}, 2$. In Figure 5 the ratio of the P to S energy densities E_P/E_S is plotted as a function of time in terms of the mean free time of the shear waves $\tau_S = l_S/\beta$. The results are shown for an isotropic source of shear waves and a source station distance of two P mean free paths. After a transition regime, we find that the P and S energies equilibrate exactly with the expected ratio. Our numerical simulations show some oscillations caused by an incomplete averaging. The characteristic time required to reach equipartition is about 25 shear mean free times, which is rather large. One should note that as the ratio α/β changes, the angular dependence of the differential cross sections is modified. This clearly shows that the details of the scattering are unimportant and that only the P and S speeds affect the ratio E_P/E_S at equilibrium. Scattering just ensures the coupling between P and S modes and equipartition in the whole phase space. We stress that the ratio of the P to S energy densities calculated with the SSc approximation does not tend to a constant. Therefore, if the equilibration could be observed, the SSc approximation may be discarded as a physical explanation for the coda, leaving the alternative of a coda composed of diffuse waves.

7. Comparison of the Rayleigh-Gans and Rayleigh Regimes

7.1. Scattering Characteristics

In Figures 6a-6d we show the polar diagrams of the differential scattering cross sections for one sphere in the

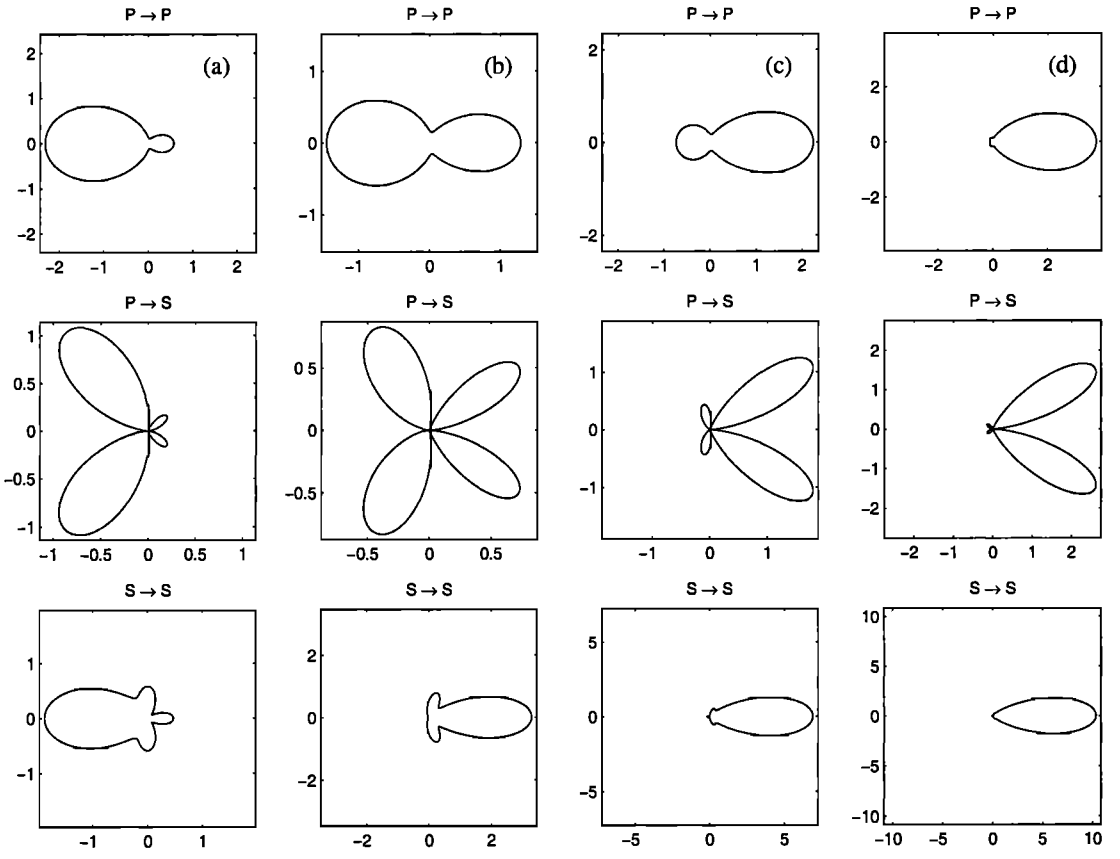

Figure 6. Polar plot of the differential scattering cross sections for the mode conversions P-P, P-S and S-S for (a) Rayleigh regime $k_P a \ll 1$, (b) Rayleigh-Gans (R-G) regime $k_P a = 1.2$, (c) R-G regime $k_P a = 1.6$, and (d) R-G regime $k_P a = 2$

Rayleigh-Gans and Rayleigh regimes. For S-S scattering, we averaged over the azimuthal angle Φ, which corresponds to incident depolarized waves. In the Rayleigh regime, scatterers are taken to be significantly smaller than the wavelength ($k_P a \ll 1$). In this case, most part of the energy is scattered in the backward direction, as shown in Figure 6a. In multiple scattering, this feature tends to keep the energy close to the source. A typical consequence of this situation is that the transport mean free paths $l_P^\star$ and $l_S^\star$ are smaller than the scattering ones. We note that the ratio l_P/l_S of the mean free paths is rather large (2.6), which means that scattering is much stronger for S waves than for P waves.

In the Rayleigh-Gans regime (Figures 6b-6d), the scatterers are supposed to be of a size that is comparable to the wavelength ($k_P a \sim 1$). As $k_P a$ increases, the angular dependence of the scattering becomes more and more anisotropic, and the P-P and S-S differential cross sections start to exhibit a peak in the forward direction, as also known to occur for acoustic waves [*Chernov*, 1960]. The ratio l_P/l_S varies from 1.5 to 2, but the enhanced forward scattering causes the transport mean free paths to become much larger than the scattering mean free paths. For example, for $k_P a = 2$ we find $l_S^\star \simeq 4.6 l_S$ and $l_P^\star \simeq 2.5 l_P$. Most of the scattered energy is concentrated in a small solid angle in the forward direction, and therefore several scatterings are required before the scattered waves loose memory of their initial direction. All the characteristics of the Rayleigh and Rayleigh-Gans scattering have been summarized in Table 1. For all values of ka, S-P or P-S conversions are forbidden in the exact forward and backward directions. From this brief description we conclude that the scattering mechanism heavily depends on the size of the scatterers as compared to the wavelength and therefore expect different behaviors regarding the shape of the envelopes and the convergence to diffusion and energy equilibration. These topics will be discussed in section 8.

7.2. Analysis of the Synthetic Codas

In Figure 7 we present the results of our numerical simulations in the Rayleigh regime. Figure 7 is composed of three parts. In Figure 7(top) we show the P (solid lines) and S (dashed lines) energy densities as a function of time. On each horizontal axis, time is expressed in terms of the shear mean free time. In Figure 7(middle) the total energy density $E_P + E_S$ is plotted in solid lines and compared to the solution of the diffu-

$k_P a \ll 1$

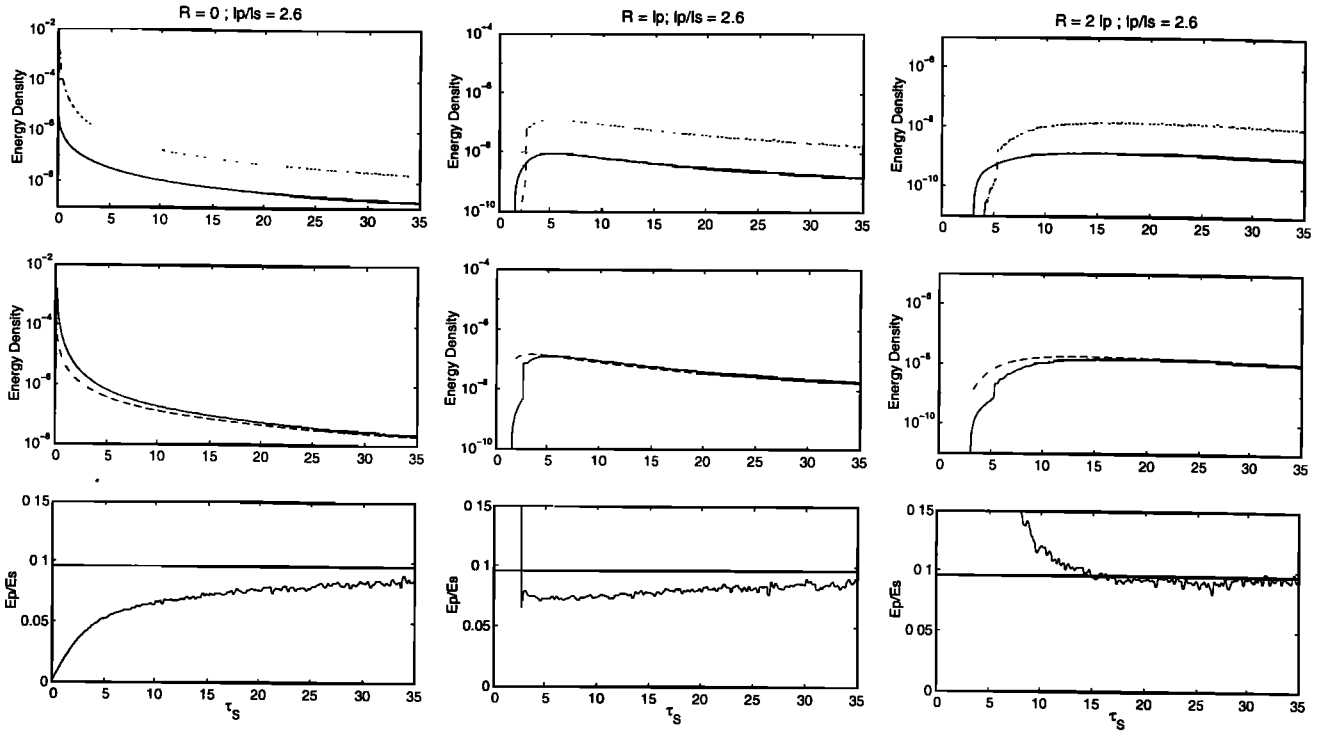

Figure 7. Results of the Monte Carlo simulation for an isotropic and point-like source of S waves in a medium with Rayleigh scatterers. The ratio l_P/l_S and the source-station distance R (in terms of P mean free path) are indicated at the top. Time is indicated on the horizontal axis in term of the S mean free time. (Top) Energy density of the S waves (dashed) and of the P waves (solid). (Middle) Comparison of the total energy density (solid) with the diffusion approximation (dashed). (Bottom) Plot of the E_P/E_S ratio. The theoretical asymptotic value is also indicated.

sion equation in dash-dotted lines. This enables us to discuss the accuracy of the diffusion approximation. In Figure 7(bottom) the ratio of S to P energy densities is plotted. Note that Figure 7(bottom) has no logarithmic scale, which makes the evaluation of the equilibration time easier. We recall that in all our simulations we have $l_S = 30$ km. As explained in section 6, choosing another value of l_S in the simulations would just result in changing the absolute value of the energy density.

In the Rayleigh regime $k_P a \ll 1$, most of the energy is backscattered (see Figure 6a). Except when source and receivers are close (typically less than one transport mean free path), the synthetic codas are rather smooth, showing a slow evolution of the energy density with time. The smoothness of the curves reflects that in the Rayleigh regime ($k_P a \ll 1$) the angular dependence of the scattering is only slightly anisotropic as compared to the Rayleigh-Gans regime. At a few mean free paths from the source the maximum of the total energy density occurs after the arrival time of the primary waves. Beyond this maximum, the energy of the coda is almost flat. A similar behavior is observed in the acoustic case for isotropic scatterers [*Margerin et al.*, 1998] and shows the formation of a diffusion front. This is confirmed by the very good agreement between the diffusion approximation and the simulation. We note that for elastic waves the transport mean free paths can be smaller than the scattering one. This can never be achieved for acoustic waves. In particular, in the Rayleigh regime of acoustic waves, scattering becomes isotropic.

Figure 8 shows the results of our computations for Rayleigh-Gans scattering with ($k_P a = 1.6$). The energy arrival associated with the forward scattered waves can clearly be identified. Just after this peak, the energy falls by 1 order of magnitude and then decays slowly, exactly as predicted by the diffusion approximation. The analytical form ($\sim t^{-3/2}$) of the coda in the diffusion regime is very simple. By comparing Figures 7 and 8 we can observe that the diffusive regime is reached much more rapidly for Rayleigh-Gans scattering than for Rayleigh scattering. Several reasons can be invoked to explain this result. As has already been pointed out by *Turner* [1998], a large value of the ratio l_P/l_S tends to delay the diffusion regime. This statement is confirmed by our computations. In spite of the larger P wave velocity the shear mean free time is smaller than the compressional one. This means that the time re-

Table 1. Scattering Parameters in Different Regimes

	$\frac{\Sigma_{PP}}{\Sigma_{PS}}$	$\frac{\Sigma_{SS}}{\Sigma_{SP}}$	$\frac{l_P}{l_S}$	$\frac{l_S^*}{l_S}$	$\frac{l_P^*}{l_P}$	$\frac{\Sigma_{PP}^*}{\Sigma_{PP}}$	$\frac{\Sigma_{PS}^*}{\Sigma_{PS}}$	$\frac{\Sigma_{SS}^*}{\Sigma_{SS}}$
Rayleigh regime	0.3	19.6	2.6	0.7	0.8	-0.4	-0.4	-0.3
Rayleigh-Gans regime								
$k_P a = 1.2$	0.7	14.1	1.5	1.7	0.9	-0.1	-0.1	0.4
$k_P a = 1.6$	1.2	21.2	1.67	3.1	1.5	0.2	0.5	0.7
$k_P a = 2.0$	1.2	28.4	2.0	4.6	2.5	0.6	0.7	0.8

quired to achieve isotropy and equipartition for P waves is expected to be larger than for S waves. In addition, we note that for Rayleigh scattering, P waves are preferentially converted into S waves (see Table 1). This means that the P mode is rather unstable, which prevents the onset of a rapid equilibration between the P and S energies. This is illustrated by the slow evolution of the ratio E_P/E_S in Figure 7, where equipartition is reached after at least 15 mean free times. For Rayleigh-Gans scatterers (Figure 8), only five mean free times or less are required. In this case, there is a very efficient coupling between the P and S modes.

A remarkable result is the effect of the source station distance R on the equilibration time. In Figure 7 and 8, we note that the largest timescale occurs when the source and the receiver are close. This is particularly evident in the Rayleigh case where the onset of equilibration takes no less than 35 mean free times. In Figure 7 we see that it takes quite a long time for the total energy density to be described very accurately by the diffusion approximation when the source station distance $R = 0$. This means that most of the energy leaves the source region before it is diffuse. The part which remains corresponds to the energy which propagates slowly, far behind the diffusion front, and that is not equilibrated. This effect is more pronounced in the Rayleigh case because of the difference in the P and S scattering mean free paths. As the source-station distance increases, the energy that arrives at the receiver rapidly exhibits a diffusive behavior as has been described above. Therefore the time evolution of the E_P/E_S ratio could be used to discriminate different scattering mechanisms, which are determined by the size of the scatterers compared to the wavelength. Although in some cases equipartition can be quite long to achieve, we find that the solution of the diffusion equation approximates the full solution rather well. This suggests that the coda could be accurately described in the framework of the diffusion theory, as has already been proposed by *Campillo et al.* [1999]. It is also noticeable that the value of equipartition is com-

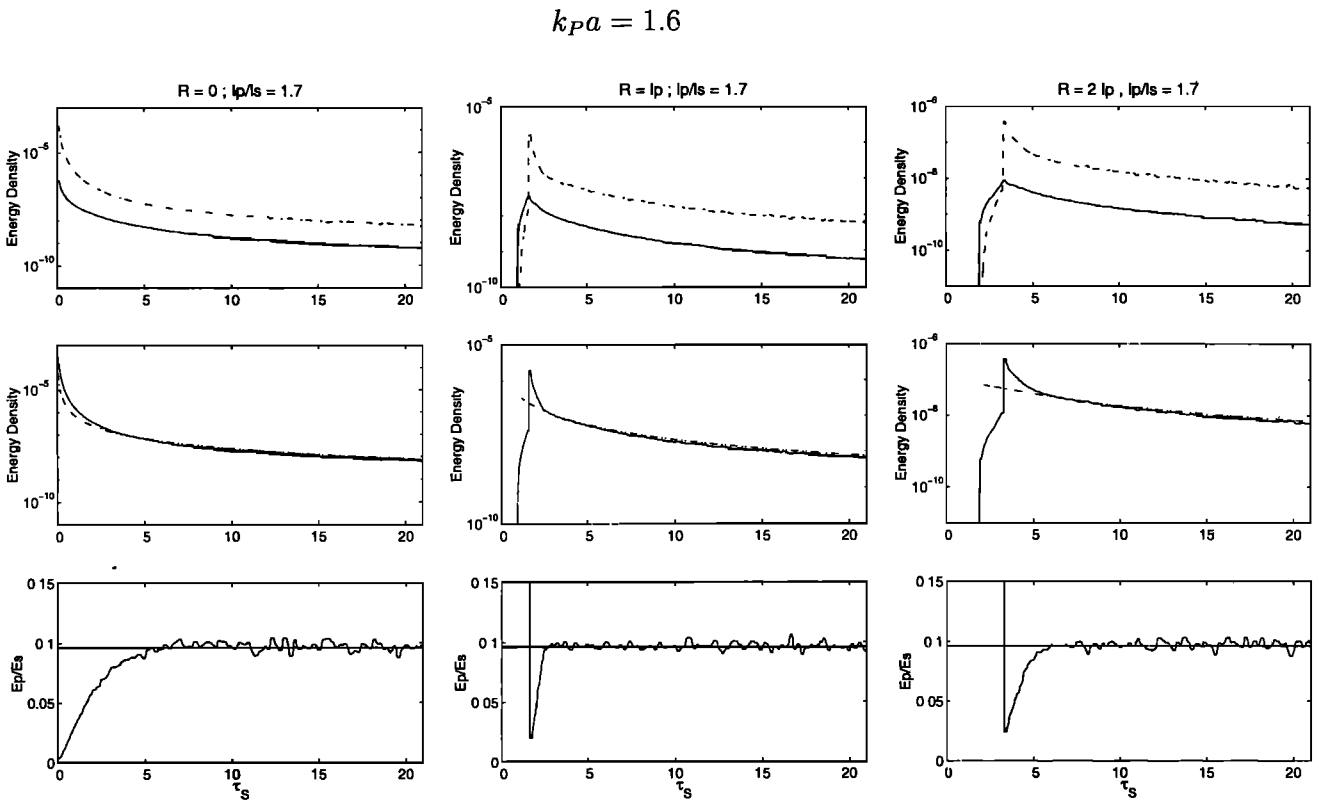

Figure 8. Same as Figure 7 with R-G scatterers ($k_P a = 1.6$)

$k_P a = 1.2$

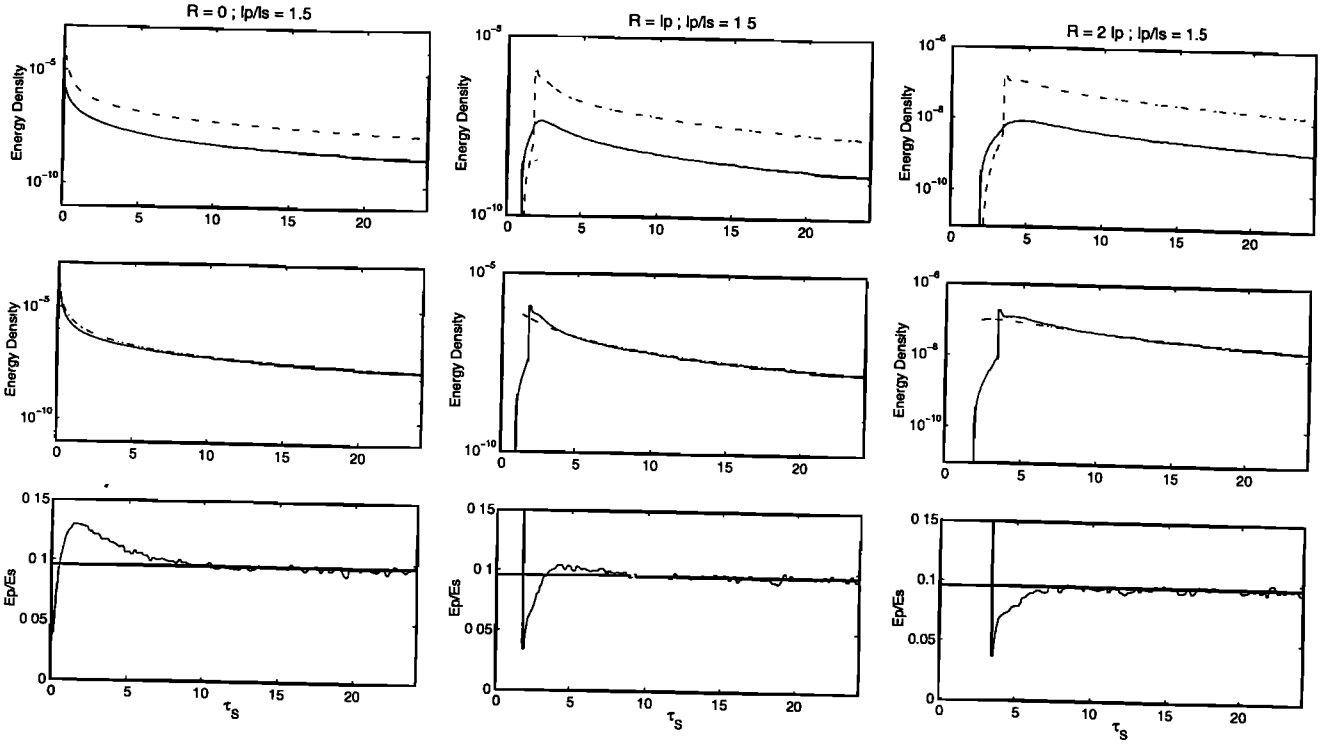

Figure 9. Same as Figure 7 with $k_P a = 1.2$

pletely independent of the scattering mechanism and only depends on the ratio α/β.

Even though the multiple-scattering field is found to converge to a universal regime, we find, for early times, a strong dependence of the shape of the energy envelopes on the scattering mechanism. This can be most easily appreciated when we consider receivers located at a few mean free paths from the source. In Figure 7 the envelope is spindle shaped, as can be observed on lunar records. When scattering is predominantlly forward, as is the case in Figure 8, the shape of the envelope is rather impulsive and exhibits broadening with increasing distance. Recently, *Gusev and Abubakirov* [1999a, b] have proposed using the shape of the energy envelopes at early times to infer the depth dependence of the scattering mean free paths. Their approach is based on the often observed envelope-broadening phenomenon but does not incorporate the mode conversions. While an interesting problem, it is beyond the scope of this paper to discuss how envelope broadening of elastic waves depends on different scattering mechanisms. Hereinafter, we shall rather focus on the approach to equilibration.

8. Diffusion and Equilibration

In this section we discuss the parameters that can affect the equilibration time. In Figure 9 and Figure 10, we present the results of the Monte Carlo simulations in the Rayleigh-Gans regime ($k_P a = 1.2$ and $k_P a = 2$) for a source of linearly polarized shear waves. We recall that as $k_P a$ increases, the scattering becomes more and more anisotropic and forwardly peaked as illustrated by the polar plots of the differential scattering cross sections in Figure 6. The case $k_P a = 2$ is very similar to $k_P a = 1.6$ except that the equilibration time is largely delayed. This follows from the increase of the ratio l_P/l_S, as discussed above, and from the highly anisotropic angular dependence of the scattering. When l_P is much larger than l_S, the P energy can propagate on large distances without being significantly scattered. Moreover, when the angular dependence of the scattering is highly anisotropic, the transport mean free paths are much larger than the scattering mean free paths. Thus complete isotropy of the field will take a long time to set in.

The case $k_P a = 1.2$ is rather interesting because the scattering is preferentially forward for S waves and backward for P waves. Although the l_P/l_S ratio is smaller (about 1.5) in this case, the equilibration time is somewhat larger than for $k_P a = 1.6$, especially at short offsets. This suggests that the ratio l_P/l_S is not the only parameter that controls the equilibration time. In Figure 9 we note that the time variation of the ratio E_P/E_S exhibits an overshoot which disappears as the receiver is moved away from the source. This can be explained by the fact that the P wave energy tends to remain close to the source, while the S wave energy is scattered away. Once again, we note that the study of

$k_P a = 2$

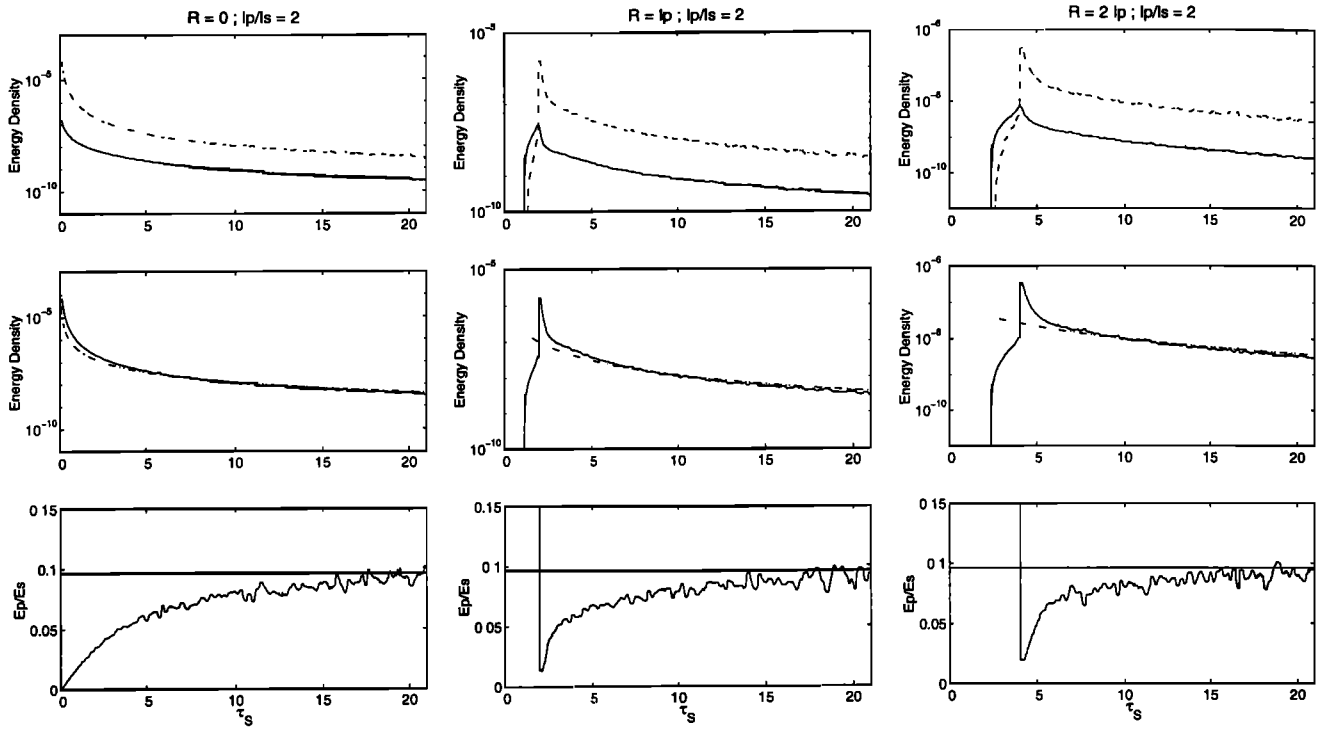

Figure 10. Same as Figure 7 with $k_P a = 2$

the E_P/E_S ratio could provide useful information concerning the scattering mechanism in the Earth.

A final comment will be on the effect of the source. In Figure 11 we show the results of the numerical simulation for $k_P a = 1.2$ and $k_P a = 1.6$, with an isotropic source of P energy. The situation is now the opposite to the one with an S source. Equipartition is reached more rapidly for $k_P a = 1.2$ than for $k_P a = 1.6$ where the equilibrium between the P and S energies is delayed by a factor of 2. This has also been observed for ultrasounds by *Turner and Weaver* [1994c]. To explain the effect of the source, we must consider the higher value of the l_P/l_S ratio for $k_P a = 1.6$ which enables the P energy to propagate on larger length without being significantly scattered. Also in this case, $\Sigma_{PP} > \Sigma_{PS}$ (see Table 1) implies that P waves are preferentially scattered into P waves, which is unfavorable for the equilibration of the energy. The numerical simulations for P sources in the Rayleigh regime have shown no influence on the equilibration time because in this case the P energy is almost completely converted into shear energy after a few scatterings.

9. Conclusion and Outlook

Our numerical simulations have shown that in the coda, S energy rapidly dominates, independent of the nature of the source and consistent with the equipartition principle. With our choice of scattering parameters the single-scattering approximation leads to exactly the opposite statement. Another fundamental difference concerns the evolution of the ratio E_P/E_S with time. When multiple scattering is taken into account, the energy density ratio E_P/E_S stabilizes in a universal way, as theoretically predicted by *Weaver* [1990] and *Ryzhik et al.* [1996]. An observation of the time evolution of the E_P/E_S ratio would help to identify the physical process responsible for the formation of the coda. An experimental procedure to measure the E_P/E_S ratio has been recently proposed by *Campillo et al.* [1999] and N. M. Shapiro et al. (The energy partitioning between P and S waves and the diffusive chaacter of the seismic coda, submitted to *Bulletin of the Seismological Society of America,* 1999) based on the separation of the wave field in its rotational and divergence components. Preliminary observations by these authors strongly suggest that equipartion can be observed on actual data in Mexico.

Although the E_P/E_s ratio tends to a constant, the equilibration time heavily depends on the scattering mechanisms. With our choice of model parameters we find that for Rayleigh scatterers, no less than 15 mean free times are required to reach equipartion. The main reason for this is the large value of the P mean free path. P energy propagates on rather large distances without having scattered significantly. This conclusion is in agreement with *Turner and Weaver* [1994b,c]. On the other hand, in the Rayleigh-Gans regime, equipar-

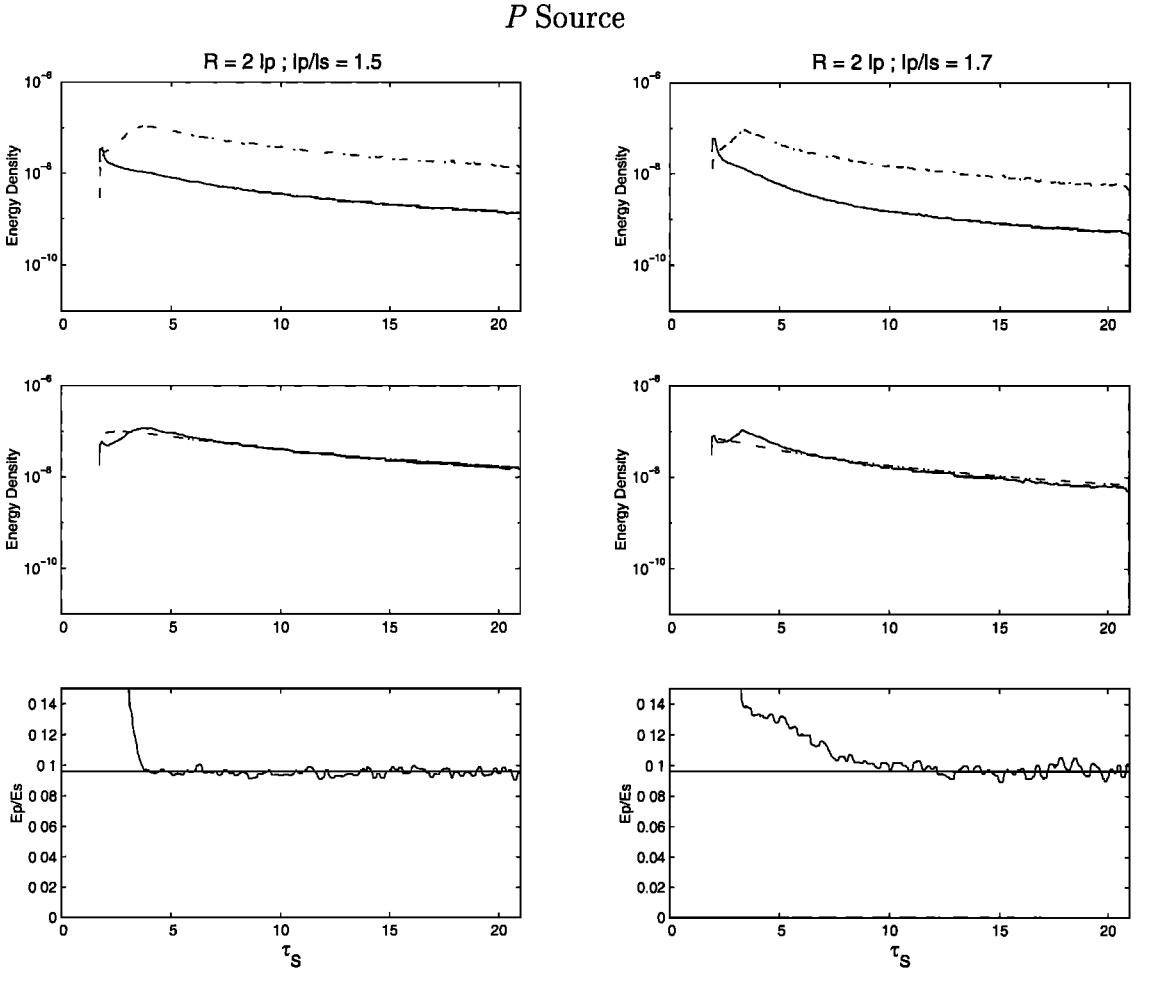

Figure 11. Same as Figure 7 with a P wave source emitting in a medium with Rayleigh-Gans scatterers.

tition can be reached very rapidly, within a few mean free times. Although the differential cross section is more anisotropic in this case, the l_P/l_S ratio is closer to 1, which ensures an efficient coupling between the two modes. As $k_P a$ increases, the scattering becomes more and more anisotropic, which tends to postpone the equilibration. The effect of the source station distance has also been studied. When source and receivers are close, equilibration is also delayed. On the other hand, as the source-station distance increases, the field becomes rapidly diffuse after the arrival of the primary waves. Therefore, if the offset amounts a few mean free paths, the equilibration of the P and S modes could be observed. The use of a P source also delays the equilibration time, especially in the Rayleigh-Gans regime, but this effect is weaker than the one of the source-station distance. The measurement of the E_P/E_S ratio could be used as a marker of the scattering mechanisms in the Earth.

Additional difficulties have to be overcome to model the propagation of high-frequency waves in the lithosphere. First, we have to take into account the boundary reflections at the free surface and the Moho, which will introduce conversions of the P and S modes. Second, most seismic experiments are set up at the free surface of the Earth. The reflection at the surface introduces deterministic interferences between the incident and reflected waves, which are neglected in the classical theory of radiative transfer. An important task for future studies will be to incorporate the mode conversions and deterministic interference effects.

Appendix A: Rotation of the Stokes Parameters

Let us define a Cartesian reference frame $(\mathbf{x_0}, \mathbf{y_0}, \mathbf{z_0})$. If this frame is rotated an angle ϕ in the positive sense around the z_0 axis, one obtains the new reference frame $(\mathbf{x}, \mathbf{y}, \mathbf{z_0})$. Simple geometrical relations and the application of the definition of the Stokes parameters (3a)-(3e) lead to the matrix $\mathbf{L}$ given in (7) that relates original and rotated Stokes vectors.

$$\mathbf{L}(\phi) = \begin{pmatrix} 1 & 0 & 0 & 0 & 0 \\ 0 & \cos^2\phi & \sin^2\phi & \frac{1}{2}\sin 2\phi & 0 \\ 0 & \sin^2\phi & \cos^2\phi & -\frac{1}{2}\sin 2\phi & 0 \\ 0 & -\sin 2\phi & \sin 2\phi & \cos 2\phi & \\ 0 & 0 & 0 & 0 & 1 \end{pmatrix}. \quad \text{(A1)}$$

Appendix B: Functions f and γ in the Rayleigh-Gans Approximation

Let us introduce perturbations of the Lamé parameters $\delta\lambda$, $\delta\mu$ and of the density $\delta\rho$ with respect to the homogeneous reference medium; α and β refer to the P wave and S wave speeds, respectively. It is shown by *Wu and Aki* [1985a] using the Born approximation that the effect of an elastic inhomogeneity can be represented by equivalent body forces and a moment tensor. More precisely, the scattered wave field U_i reads

$$U_i = F_j * G_{ij} + M_{jk} * G_{ij,k}, \quad \text{(B1)}$$

where i, j, k denote space directions, F_j is the equivalent body forces, G_{ij} is the elastic Green tensor, M_{jk} is the equivalent moment tensor, and the star $*$ is the convolution symbol. The difference between our results and those of *Wu and Aki* [1985a] is purely formal due to a different choice of coordinate system for S wave incidence. They define the polar axis as the direction of particle motion, whereas we define the polar axis as the propagation direction of the incident wave. Fortunately, our result for S wave scattering takes a simpler form than *Wu and Aki's* [1985a] form.

Let us first discuss Rayleigh scattering. In this case the perturbations can be considered to be point-like. The scattering geometry and notation conventions are depicted in Figure 1. The incident S wave propagates in the $\mathbf{z}$ direction and has particle motion along the $\mathbf{x}$ direction, with unit amplitude. The scattered wave propagates in the $\mathbf{p}'$ direction with direction cosines: $p'_x = \sin\Theta\cos\Phi$, $p'_y = \sin\Theta\sin\Phi$, $p'_z = \cos\Theta$. Using the representation (B1) and following *Wu and Aki* [1985a], one obtains the far-field scattered P wave displacements in the x, y, z frame:

$$\mathbf{U_{SP}} = \frac{\omega^2 V}{4\pi\alpha^2 r}\exp\left[-i\omega(t - r/\alpha)\right] \times \begin{pmatrix} p_x'^2\frac{\delta\rho}{\rho} - 2p_x'^2 p'_z\frac{\beta}{\alpha}\frac{\delta\mu}{\mu} \\ p'_x p'_y\frac{\delta\rho}{\rho} - 2p'_x p'_y p'_z\frac{\beta}{\alpha}\frac{\delta\mu}{\mu} \\ p'_x p'_z\frac{\delta\rho}{\rho} - 2p'_x p_z'^2\frac{\beta}{\alpha}\frac{\delta\mu}{\mu} \end{pmatrix}, \quad \text{(B2)}$$

where V is the volume of the inclusion and r is the distance to the observer. V is assumed to be very small, and r is assumed to be very large, as compared to the wavelength; t is time and ω is the angular frequency of the wave. Similarly, one obtains the scattered S wave displacements in the $(\mathbf{x}, \mathbf{y}, \mathbf{z})$ frame:

$$\mathbf{U_{SS}} = \frac{\omega^2 V}{4\pi\beta^2 r}\exp\left[-i\omega(t - r/\beta)\right] \times \begin{pmatrix} (1 - p_x'^2)\frac{\delta\rho}{\rho} + p'_z(2p_x'^2 - 1)\frac{\delta\mu}{\mu} \\ -p'_x p'_y\frac{\delta\rho}{\rho} + 2p'_x p'_y p'_z\frac{\delta\mu}{\mu} \\ -p'_x p'_z\frac{\delta\rho}{\rho} + p'_x(2p_z'^2 - 1)\frac{\delta\mu}{\mu} \end{pmatrix}. \quad \text{(B3)}$$

The next step consists of rotating the displacement vectors onto the local spherical frame $(\mathbf{r}', \mathbf{l}', \mathbf{p}')$. After some straightforward calculations we find the displacement vectors in the local spherical frame. For the sake of simplicity, we use the same notations to represent the wave displacements in the new frame. We obtain

$$\mathbf{U_{SP}} = \frac{\cos\Phi\omega^2 V}{4\pi\alpha^2 r}\exp\left[-i\omega(t - r/\alpha)\right] \times \begin{pmatrix} \sin\Theta\frac{\delta\rho}{\rho} - 2\frac{\beta}{\alpha}\frac{\delta\mu}{\mu}\sin\Theta\cos\Theta \\ 0 \\ 0 \end{pmatrix} \quad \text{(B4)}$$

for the scattered P wave and

$$\mathbf{U_{SS}} = \frac{\omega^2 V}{4\pi\beta^2 r}\exp\left[-i\omega(t - r/\beta)\right] \times \begin{pmatrix} 0 \\ \left[\frac{\delta\rho}{\rho}\cos\Theta + \frac{\delta\mu}{\mu}(1 - 2\cos^2\Theta)\right]\cos\Phi \\ \left[-\frac{\delta\rho}{\rho} + \frac{\delta\mu}{\mu}\cos\Theta\right]\sin\Phi \end{pmatrix} \quad \text{(B5)}$$

for the scattered S wave. It is apparent that with our conventions the Θ and Φ dependences separate. It is thus very easy to identify the functions f_* introduced in (9) and describing the angular dependence of the scattered field for Rayleigh scattering. For completeness, we give these functions for both P and S wave incidence:

$$f_{PP}(\Theta) = -\frac{\delta\lambda}{\lambda + 2\mu} + \frac{\delta\rho}{\rho}\cos\Theta - \frac{2\delta\mu}{\lambda + 2\mu}\cos^2\Theta \quad \text{(B6)}$$

$$f_{PS}(\Theta) = \left(\frac{2\beta}{\alpha}\right)\frac{\delta\mu}{\mu}\sin\Theta\cos\Theta - \frac{\delta\rho}{\rho}\sin\Theta \quad \text{(B7)}$$

$$f_{SP}(\Theta) = -\left(\frac{2\beta}{\alpha}\right)\frac{\delta\mu}{\mu}\sin\Theta\cos\Theta + \frac{\delta\rho}{\rho}\sin\Theta \quad \text{(B8)}$$

$$f_{SS_l}(\Theta) = \frac{\delta\rho}{\rho}\cos\Theta + \frac{\delta\mu}{\mu}(1 - 2\cos^2\Theta) \quad \text{(B9)}$$

$$f_{SS_r}(\Theta) = -\frac{\delta\rho}{\rho} + \frac{\delta\mu}{\mu}\cos\Theta. \quad \text{(B10)}$$

For acoustic waves, Rayleigh scattering would be isotropic. We note that the scattering matrix depends on the polar angle Θ only. Indeed, by convention, this matrix relates the incident wave field expressed in the frame $(\mathbf{r}, \mathbf{l}, \mathbf{p})$ to the scattered wave field expressed in the frame $(\mathbf{r}', \mathbf{l}', \mathbf{p}')$ (see Figure 1). When the incident wave field is rotated from the frame $(\mathbf{x}, \mathbf{y}, \mathbf{z})$ onto the frame $(\mathbf{r}, \mathbf{l}, \mathbf{p})$, the Φ dependence disappears. The scattering cross sections are very easily obtained using the definitions given by *Sato and Fehler* [1998].

In the Rayleigh-Gans approximation (termed Mie-Born approximation by *Wu and Aki* [1985a]), finite size heterogeneities are considered as Rayleigh scatterers distributed in a volume V. Our treatment for homogeneous spheres exactly follows Wu and Aki and we refer to their original paper for a full derivation. We just outline the physical assumptions underlying this approach. The scattered wave is considered as the superposition of the partial waves produced by each small portion of the scattering volume. The phase difference between these partial waves is taken into account. The validity of this approximation is discussed by *Van de Hulst* [1981] and *Korneev and Johnson* [1993b]. In incorporating the interferences between the partial waves the functions describing the angular dependence of Rayleigh-Gans scattering take the general form $f_*(\Theta)\gamma_n(\Theta)$, where f_* denotes any of the functions defined in (B6)-(B10) and the γ_n are "shape factors" defined below. If the inclusion is a sphere of radius a with correlated homogeneous variations of the elastic parameters λ, μ, ρ, one has

$$\gamma_n(\Theta) = \frac{4\pi a^3}{(\omega S_n a)^2}\left[\frac{\sin\omega S_n a}{\omega S_n a} - \cos\omega S_n a\right] \quad \text{(B11)}$$

$$S_1(\Theta) = \frac{2}{\alpha}\sin\frac{\Theta}{2} \quad \text{(B12)}$$

$$S_2(\Theta) = \sqrt{\left(\frac{1}{\alpha}\right)^2 + \left(\frac{1}{\beta}\right)^2 - \frac{2}{\alpha\beta}\cos\Theta} \quad \text{(B13)}$$

$$S_3(\Theta) = S_2(\Theta) \quad \text{(B14)}$$

$$S_4(\Theta) = \frac{2}{\beta}\sin\frac{\Theta}{2}. \quad \text{(B15)}$$

In the acoustic case, the functions γ_1 and S_1 suffice to derive the shape factor.

Appendix C: Mueller Matrix for a Spherical Scatterer

Consider a plane wave incident on a scatterer in the direction (θ', ϕ') and scattered into the direction (θ, ϕ), where the directions are given in usual polar coordinates. The angle between both directions will be denoted Θ. The relation between the scattering matrix $\mathbf{F}$ and the Mueller matrix $\mathbf{P}$ is

$$\mathbf{P} = \mathbf{L}(i_2 - \frac{3\pi}{2})\mathbf{F}(\Theta)\mathbf{L}(i_1 + \frac{\pi}{2}), \quad \text{(C1)}$$

where $\mathbf{L}$ is the rotation matrix given in Appendix A and i_1 and i_2 are defined by the following trigonometric relations:

$$\cos i_1 = \frac{1}{\sqrt{1-\cos^2\Theta}}\left[\cos\theta\sqrt{1-\cos^2\theta'} - \cos\theta'\sqrt{1-\cos^2\theta}\cos(\phi'-\phi)\right] \quad \text{(C2)}$$

$$\sin i_1 = \sqrt{\frac{1-\cos^2\theta}{1-\cos^2\Theta}}\sin(\phi'-\phi) \quad \text{(C3)}$$

$$\cos i_2 = \frac{1}{\sqrt{1-\cos^2\Theta}}\left[\cos\theta'\sqrt{1-\cos^2\theta} - \cos\theta\sqrt{1-\cos^2\theta'}\cos(\phi'-\phi)\right] \quad \text{(C4)}$$

$$\sin i_2 = \sqrt{\frac{1-\cos^2\theta'}{1-\cos^2\Theta}}\sin(\phi'-\phi). \quad \text{(C5)}$$

We recall that

$$\cos\Theta = \sqrt{1-\cos^2\theta}\sqrt{1-\cos^2\theta'}\cos(\phi-\phi') + \cos(\theta)\cos(\theta').$$

In order to simplify the final expressions, we introduce the following functions:

$$F_{PP}(\Theta) = f_{PP}(\Theta)\gamma_1(\Theta)$$
$$F_{PS}(\Theta) = f_{PS}(\Theta)\gamma_2(\Theta)$$
$$F_{SP}(\Theta) = f_{SP}(\Theta)\gamma_3(\Theta)$$
$$F_{SS_l}(\Theta) = f_{SS_l}(\Theta)\gamma_4(\Theta)$$
$$F_{SS_r}(\Theta) = f_{SS_r}(\Theta)\gamma_4(\Theta).$$

Except for a constant prefactor, the terms P_{ij}, where $i, j \in [1, 5]$ of the matrix P, read

$$P_{11} = k_P^4 F_{PP}^2(\Theta) \quad \text{(C6)}$$

$$P_{12} = \frac{\alpha}{\beta}k_P^4 F_{SP}^2(\Theta)\cos^2 i_1 \quad \text{(C7)}$$

$$P_{13} = \frac{\alpha}{\beta}k_P^4 F_{SP}^2(\Theta)\sin^2 i_1 \quad \text{(C8)}$$

$$P_{14} = \frac{\alpha}{2\beta}k_P^4 F_{SP}^2(\Theta)\sin 2i_1 \quad \text{(C9)}$$

$$P_{15} = 0 \quad \text{(C10)}$$

$$P_{21} = \frac{\beta}{\alpha}k_S^4 F_{PS}^2(\Theta)\cos^2 i_2 \quad \text{(C11)}$$

$$P_{22} = k_S^4 r^2 \quad \text{(C12)}$$

$$r = F_{SS_r}(\Theta)\sin i_1 \sin i_2 - F_{SS_l}(\Theta)\cos i_1 \cos i_2$$

$$P_{23} = k_S^4 s^2 \quad \text{(C13)}$$

$$s = F_{SS_r}(\Theta)\cos i_1 \sin i_2 + F_{SS_l}(\Theta)\sin i_1 \cos i_2$$

$$P_{24} = -k_S^4 rs \quad \text{(C14)}$$

$$P_{25} = 0 \quad \text{(C15)}$$

$$P_{31} = \frac{\beta}{\alpha}k_S^4 F_{PS}^2(\Theta)\sin^2 i_2 \quad \text{(C16)}$$

$$P_{32} = k_S^4 t^2 \quad \text{(C17)}$$

$$t = F_{SS_r}(\Theta)\sin i_1 \cos i_2 + F_{SS_t}(\Theta)\cos i_1 \sin i_2$$

$$P_{33} = k_S^4 u^2 \quad \text{(C18)}$$

$$u = F_{SS_r}(\Theta)\cos i_1 \cos i_2 - F_{SS_t}(\Theta)\sin i_1 \sin i_2$$

$$P_{34} = k_S^4 tv \quad \text{(C19)}$$

$$v = F_{SS_t}(\Theta)\sin i_1 \sin i_2 - F_{SS_r}(\Theta)\cos i_1 \cos i_2$$

$$P_{35} = 0 \quad \text{(C20)}$$

$$P_{41} = -\frac{\beta}{\alpha} k_S^4 F_{PS}^2(\Theta)\sin 2i_2 \quad \text{(C21)}$$

$$P_{42} = 2k_S^4 rt \quad \text{(C22)}$$

$$P_{43} = 2k_S^4 su \quad \text{(C23)}$$

$$P_{44} = k_S^4(rv - st) \quad \text{(C24)}$$

$$P_{45} = 0 \quad \text{(C25)}$$

$$P_{51} = 0 \quad \text{(C26)}$$

$$P_{52} = 0 \quad \text{(C27)}$$

$$P_{53} = 0 \quad \text{(C28)}$$

$$P_{54} = 0 \quad \text{(C29)}$$

$$P_{55} = k_S^4 F_{SS_r}(\Theta) F_{SS_t}(\Theta) \quad \text{(C30)}$$

One may check that this matrix has all the symmetry properties discussed by *Sekera* [1966] and *Turner and Weaver* [1994a].

Appendix D: Scattering Cross Sections in the Rayleigh Regime

The scattering cross section are defined by

$$\Sigma_{MN} = \int_{4\pi} \frac{d\sigma_{MN}}{d\Omega} d\Omega, \quad \text{(D1)}$$

where 4π denotes the whole sphere of space directions and $d\Omega$ is an element of solid angle. After straightforward calculations, we find

$$\Sigma_{PP} = \frac{V^2 k_P^4}{4\pi}\left[\left(\frac{\delta\lambda}{\lambda+2\mu}\right)^2 + \frac{4}{5}\left(\frac{\delta\mu}{\lambda+2\mu}\right)^2 + \frac{1}{3}\left(\frac{\delta\rho}{\rho}\right)^2 + \frac{4}{3}\frac{\delta\lambda\delta\mu}{(\lambda+2\mu)^2}\right] \quad \text{(D2)}$$

$$\Sigma_{PS} = \frac{V^2 k_S^4 \beta}{2\pi\alpha}\left[\frac{4}{15}\left(\frac{\beta}{\alpha}\right)^2\left(\frac{\delta\mu}{\mu}\right)^2 + \frac{1}{3}\left(\frac{\delta\rho}{\rho}\right)^2\right] \quad \text{(D3)}$$

$$\Sigma_{SP} = \frac{V^2 k_P^4 \alpha}{4\pi\beta}\left[\frac{4}{15}\left(\frac{\beta}{\alpha}\right)^2\left(\frac{\delta\mu}{\mu}\right)^2 + \frac{1}{3}\left(\frac{\delta\rho}{\rho}\right)^2\right] \quad \text{(D4)}$$

$$\Sigma_{SS} = \frac{V^2 k_S^4}{4\pi}\left[\frac{2}{3}\left(\frac{\delta\rho}{\rho}\right)^2 + \frac{2}{5}\left(\frac{\delta\mu}{\mu}\right)^2\right]. \quad \text{(D5)}$$

Acknowledgments. The authors would like to thank J. Turner, G. Papanicolaou, L. Ryzhik, G. Bal, and R. Maynard for helpful disccusions. We thank the Associate Editor and the reviewers for useful comments on the paper. This work was supported by CNRS through program "Intérieur de la Terre" of INSU and PRIMA research group.

References

Abubakirov, I.R., and A.A. Gusev, Estimation of scattering properties of lithosphere of Kamtchatka based on Monte-Carlo simulation of record envelope of a near earthquake, *Phys. Earth Planet. Inter.*, *67*, 52-67, 1990.

Aki, K., Scattering conversions P to S versus S to P, *Bull. Seismol. Soc. Am.*, *82*, 1969-1972, 1992.

Campillo, M., L. Margerin, and N.M. Shapiro, Seismic wave diffusion in the earth lithosphere, in *Diffuse Waves in Complex Media, NATO Sci. Ser.*, vol. 531, edited by J.P. Fouque, pp.383-404, Kluwer, Dordrecht, The Netherlands, 1999.

Chandrasekhar, S., *Radiative Transfer*, Dover, Mineola, N.Y., 1960.

Chernov, L.A., *Wave Propagation in a Random Medium*, McGraw-Hill, N.Y., 1960.

Collins, D.G., W.G. Blättner, M.B. Wells, and H.G. Horak, Backward Monte Carlo calculations of the polarization characteristics of the radiation emerging from spherical-shell atmospheres, *Appl. Opt.*, *11*, 2684-2696, 1972.

Dainty, A. M., and M.N. Töksöz, Array analysis of seismic scattering, *Bull. Seismol. Soc. Am.*, *80*, 2248-2260, 1990.

Einspruch, N.G., E.J. Witterholt, and R. Truell, Scattering of a plane transverse wave by a spherical obstacle in an elastic medium, *J. Appl. Phys.*, *31*, 806-818, 1960.

Gusev, A.A., and I.R. Abubakirov, Monte Carlo simulation of record envelope of a near earthquake, *Phys. Earth. Planet Inter.*, *49*, 30-36, 1987.

Gusev, A.A., and I.R. Abubakirov, Vertical profile of effective turbidity reconstructed from broadening of incoherent body-wave pulses, I, General approach and the inversion procedure, *Geophys. J. Int.*, *136*, 295-308, 1999a.

Gusev, A.A., and I.R. Abubakirov, Vertical profile of effective turbidity reconstructed from broadening of incoherent body-wave pulses, II, Application to Kamtchtka data, *Geophys. J. Int.*, *136*, 309-323, 1999b.

Heiderich, A., Diffusion multiple en milieu non linéaire ou anisotrope, Ph. D. thesis, Univ. Joseph Fourier, Grenoble, France, 1995.

Heiderich, A., R. Maynard, and B.A. Van Tiggelen, Multiple light scattering in oriented nematic liquid crystals: Monte Carlo simulations, *J. de Phys. II*, *7*, 765-792, 1997.

Holliger, K., and A. Levander, A stochastic view of lower crustal fabric based on evidence from the Ivrea zone, *Geophys. Res. Lett.*, *19*, 1153-1156, 1992.

Hoshiba, M., Simulation of multiple scattered coda wave excitation based on the energy conservation law, *Phys. Earth Planet. Inter.*, *67*, 123-136, 1991.

Hoshiba, M., Estimation of nonisotropic scattering in western Japan using coda waves envelopes: Application of a multiple nonisotropic scattering model, *J. Geophys. Res.*, *100*, 645-657, 1995.

Hoshiba, M., Seismic coda wave envelope in depth dependent S-wave velocity structure, *Phys. Earth Planet. Inter.*, *104*, 15-22, 1997.

Korneev, V.A., and L.R. Johnson, Scattering of elastic waves by a spherical inclusion, I, Theory and numerical results, *Geophys. J. Int.*, *115*, 230-250, 1993a.

Korneev, V.A., and L.R. Johnson, Scattering of elastic waves by a spherical inclusion, II, Limitations of asymptotic solutions, *Geophys. J. Int.*, *115*, 251-263, 1993b.

Korneev, V.A., and L.R. Johnson, Scattering of elastic waves by a spherically symmetric inclusion, *Pure Appl. Geophys.*, *147*, 675-718, 1996.

Lagendijk, A., and B.A. Van Tiggelen, Resonant multiple scattering of light, *Phys. Rep.*, *270*, 143-215, 1996.

Lux, I., and L. Koblinger, *Monte Carlo Particle Transport Methods: Neutron and Photon Calculations*, CRC Press, Boca Raton, Fla., 1991.

Marchuk, G.I., G.A. Mikhailov, M.A. Nazaraliev, R.A. Darbinjan, B.A. Kargin, and B.S. Elepov, *The Monte Carlo Methods in Atmospheric Optics*, Springer-Verlag, N.Y., 1980.

Margerin, L., M. Campillo, and B. Van Tiggelen, Radiative transfer and diffusion of waves in a layered medium: New insight into coda *Q*, *Geophys. J. Int.*, *134*, 596-612, 1998.

Papanicolaou, G.C., L.V. Ryzhik, and J.B. Keller, Stability of the *P*-to-*S* energy ratio in the diffusive regime, *Bull. Seismol. Soc. Am.*, *86*, 1107-1115, 1996 (Erratum, *Bull. Seismol. Soc. Am.*, *86*, 1997, 1996)

Ryzhik, L.V., G.C. Papanicolaou, and J.B. Keller, Transport equations for elastic and other waves in random media, *Wave Motion*, *24*, 327-370, 1996.

Sato, H., Attenuation of body waves and envelope formation of three-component seismograms of small local earthquakes in randomly inhomogeneous lithosphere, *J. Geophys. Res.*, *89*, 1221-1241, 1984.

Sato, H., Multiple isotropic scattering model including *P-S* conversions for the seismogram envelope formation, *Geophys. J. Int.*, *117*, 487-494, 1994.

Sato, H., and M. Fehler, *Wave Propagation and Scattering in the Heterogeneous Earth*, Springer-Verlag, New York, 1998.

Sekera, Z., Scattering matrices and reciprocity relationships for various representations of the state of polarization, *J. Opt. Soc. Am.*, *56*, 1732-1740, 1966.

Shapiro, S.A., and P. Hubral, Elastic waves in finely layered sediments: The equivalent medium and generalized O'Doherty-Anstey formulas, *Geophysics*, *65*, 1282-1300, 1996.

Turner J.A., Scattering and diffusion of seismic waves, *Bull. Seism. Soc. Am.*, *88*, 276-283, 1998.

Turner J.A., and R.L. Weaver, Radiative transfer of ultrasound, *J. Acoust. Soc. Am.*, *96*, 3654-3674, 1994a.

Turner J.A., and R.L. Weaver, Radiative transfer and multiple scattering of diffuse ultrasound in polycrystalline media, *J. Acoust. Soc. Am.*, *96*, 3675-3683, 1994b.

Turner J.A., and R.L. Weaver, Time dependence of multiply scattered diffuse ultrasound in polycrystalline media, *J. Acoust. Soc. Am.*, *97*, 2639-2644, 1994c.

Van de Hulst, H.C., *Light Scattering by Small Particles*, Dover, Mineola, N.Y., 1981.

Van Tiggelen, B.A., Localization of waves, in *Diffuse Waves in Complex Media, NATO Sci. Ser.*, vol. 531, edited by J.P. Fouque, pp.1-107, Kluwer, Dordrecht, The Netherlands, 1999.

Weaver, R.L., On diffuse waves in solid media, *J. Acoust. Soc. Am.*, *71*, 1608-1609, 1982.

Weaver, R.L., Diffusivity of ultrasound in polycrystals, *J. Mech. Phys. Solids*, *38*, 55-86, 1990.

Wu, R.S., and K. Aki, Scattering characteristics of elastic waves by an elastic heterogeneity, *Geophysics*, *50*, 582-595, 1985a.

Wu, R.S., and K. Aki, Elastic wave scattering by a random medium and the small-scale inhomogeneities in the lithosphere, *J. Geophys. Res.*, *90*, 10,261-10,273, 1985b.

Wu, R.S., Z. Xu, and X.P. Lie, Heterogeneity spectrum and scale-anisotropy in the upper crust revealed by the German Continental Deep-Drilling (KTB) holes, *Geophys. Res. Lett.*, *21*, 911-914, 1994.

Ying, C.F., and R. Truell, Scattering of a plane longitudinal wave by a spherical obstacle in an isotropically elastic solid, *J. Appl. Phys.*, *27*, 1086-1097, 1956.

Zeng, Y., Theory of scattered *P*-wave and *S*-wave energy in a random isotropic scattering medium, *Bull. Seismol. Soc. Am.*, *83*, 1264-1276, 1993.

M. Campillo, Laboratoire de Géophysique Interne, Observatoire de Grenoble, Université Joseph Fourier, BP 53X, F-38041 Grenoble Cedex, France.

L. Margerin, Department of Geosciences, Princeton University, Guyot Hall, Princeton, NJ 08544. (margerin@princeton.edu)

B. Van Tiggelen, Laboratoire de Physique et Modélisation des Systèmes Condensés, Maison des Magistères Jean Perrin CNRS, BP 66, F-38042 Grenoble Cedex, France.

(Received January 28, 1999; revised August 5, 1999; accepted October 6, 1999.)